Check for updates

JGR Atmospheres

RESEARCH ARTICLE
10.1029/2024JD042606

Atmospheric Response to Mesoscale Ocean Eddies in the Maritime Continent

Ashar A. Aslam[1], Juliane Schwendike[1], Simon C. Peatman[1,2], Adrian J. Matthews[3], Cathryn E. Birch[1], Massimo A. Bollasina[4], Paul A. Barrett[5], and Marina V. C. Azaneu[3,6]

[1]University of Leeds, Leeds, UK, [2]Now at Centre for Climate Research Singapore, Meteorological Service Singapore, Singapore, Singapore, [3]University of East Anglia, Norwich, UK, [4]University of Edinburgh, Edinburgh, UK, [5]Met Office, Exeter, UK, [6]University of New South Wales, Sydney, NSW, Australia

Key Points:

- Mesoscale ocean eddies in the Maritime Continent significantly influence surface heat flux and wind signatures
- The atmospheric response beyond the surface level, such as in cloud and rainfall, is weaker than that related to eddies in the extratropics
- Differences in properties related to both the eddies and environment may explain the reduced impact

Correspondence to:
A. A. Aslam,
eeaaas@leeds.ac.uk

Citation:
Aslam, A. A., Schwendike, J., Peatman, S. C., Matthews, A. J., Birch, C. E., Bollasina, M. A., et al. (2025). Atmospheric response to mesoscale ocean eddies in the Maritime Continent. *Journal of Geophysical Research: Atmospheres*, *130*, e2024JD042606. https://doi.org/10.1029/2024JD042606

Received 1 OCT 2024
Accepted 28 JAN 2025

Author Contributions:
Conceptualization: Ashar A. Aslam, Juliane Schwendike, Simon C. Peatman, Adrian J. Matthews, Cathryn E. Birch
Data curation: Ashar A. Aslam
Formal analysis: Ashar A. Aslam
Funding acquisition: Juliane Schwendike
Investigation: Ashar A. Aslam, Juliane Schwendike
Methodology: Ashar A. Aslam, Juliane Schwendike, Simon C. Peatman, Adrian J. Matthews
Project administration: Ashar A. Aslam, Juliane Schwendike, Simon C. Peatman
Supervision: Juliane Schwendike, Simon C. Peatman, Adrian J. Matthews, Cathryn E. Birch, Massimo A. Bollasina, Paul A. Barrett, Marina V. C. Azaneu
Visualization: Ashar A. Aslam
Writing – original draft: Ashar A. Aslam

© 2025. The Author(s).
This is an open access article under the terms of the Creative Commons Attribution License, which permits use, distribution and reproduction in any medium, provided the original work is properly cited.

Abstract Mesoscale ocean eddies contribute to the mixing and transport of water properties throughout the global ocean. Sea surface temperature anomalies associated with these eddies can influence atmospheric boundary layer stability, and thus the formation of clouds. The Maritime Continent experiences the modulation of convection and precipitation by processes operating over multiple spatial and temporal scales. However, mesoscale air-sea interactions, such as those associated with the eddies the region generates, remain understudied. Applying a sea surface height-based eddy detection and tracking algorithm, we show that lower latitude eddies, such as those in the Maritime Continent, are generally fewer in number, weaker, and shorter-lived, but larger and faster-propagating, compared to those at higher latitudes. Crucially, we highlight that eddies in the Maritime Continent can significantly modify air-sea heat exchange and the near-surface wind field. However, changes to column water vapor, cloud, and rainfall are less distinct. Compared to the Kuroshio Extension, a representative case study for the extratropics, atmospheric anomalies associated with eddies in the Maritime Continent are weaker, and decreasing in magnitude toward the lower latitudes. We hypothesize that weaker sea surface temperature anomalies associated with eddies in the Maritime Continent, coupled with their faster propagation and intraseasonal variability in convection over the region, reduce the likelihood and intensity of the instantaneous atmospheric imprint. This study therefore emphasizes the importance of the spatial and temporal scales with regard to air-sea interactions and their influence on cloud and rainfall across the Maritime Continent.

Plain Language Summary Rotating bodies of water with spatial scales of around 100 km in the surface ocean, known as mesoscale eddies, can lead to changes in ocean and lowermost atmosphere properties. Atmospheric variability in the Maritime Continent is influenced by many processes, but not much is known about the role of mesoscale ocean eddies in this region. Eddy characteristics, such as number, duration, and amplitude in sea surface height, differ between lower latitudes and higher latitudes. Signatures in the surface ocean associated with eddies, and how the atmosphere responds to them, are also weaker at lower latitudes in the Maritime Continent. These weaker responses may be due to smaller sea surface temperature anomalies, and other processes, which make the effect of the eddies harder to identify, such as their speed of propagation and atmospheric variability over the Maritime Continent.

1. Introduction

The Maritime Continent in Southeast Asia, consisting of thousands of islands and many shallow seas (Figure 1), represents a "low-latitude chokepoint" of the global oceans (Lee et al., 2019). This region is the only connection between different ocean basins in the tropics, where the Indonesian Throughflow (ITF) flows from the West Pacific Ocean to the southeast tropical Indian Ocean (Gordon, 2005; Sprintall et al., 2014). The resultant exchange and transformation of water masses in this region holds importance to the coupled ocean-atmosphere climate system (e.g., Godfrey, 1996; Makarim et al., 2019).

Tidal mixing and upwelling are dominant contributors to changes in water properties in the Maritime Continent, with vertical diffusivity in the constituent marginal seas being an order of magnitude greater than in the open ocean (Ffield & Gordon, 1996; Jochum & Potemra, 2008; Koch-Larrouy et al., 2010; Nagai et al., 2021). Mixing, primarily occurring along narrow passages or straits, is affected by the wind field, which can be modulated, for example, by the monsoon circulation and larger-scale modes of variability (e.g., Wirasatriya et al., 2021; Susanto & Ray, 2022). A key component of mixing is represented by mesoscale ocean eddies.

Writing – review & editing:
Juliane Schwendike, Simon C. Peatman, Adrian J. Matthews, Cathryn E. Birch, Massimo A. Bollasina, Paul A. Barrett, Marina V. C. Azaneu

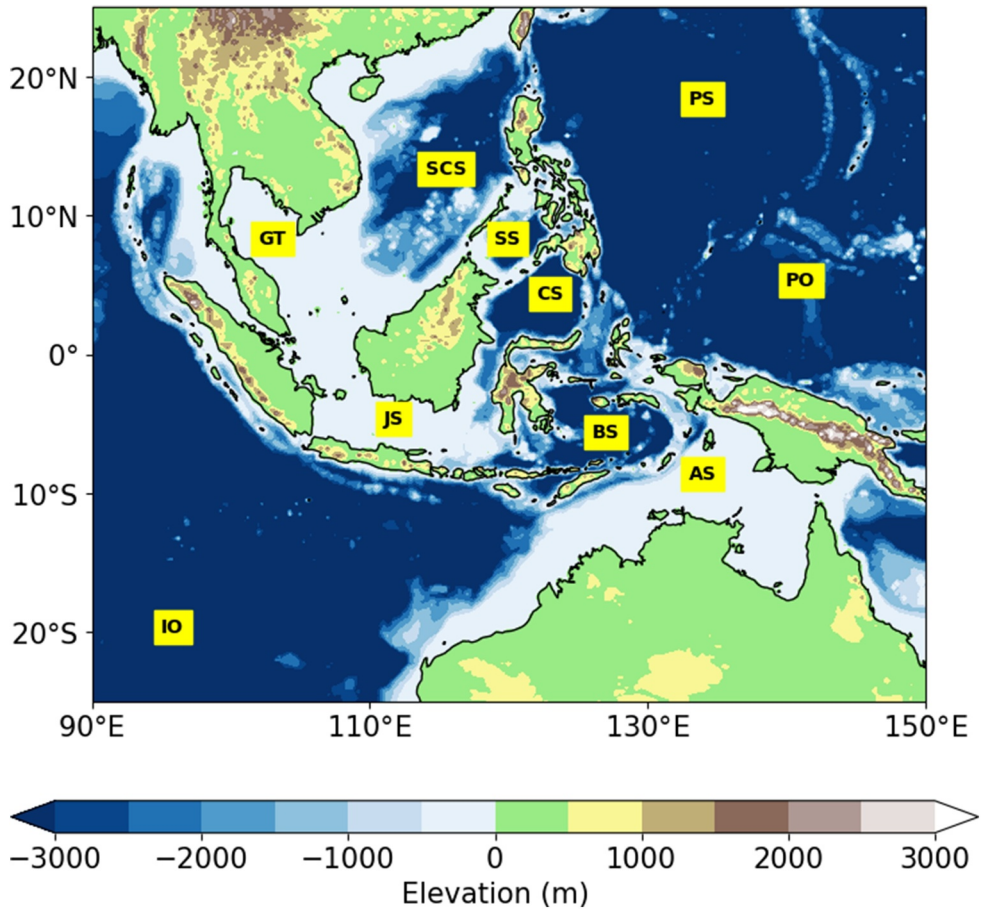

Figure 1. Map of the Maritime Continent located in Southeast Asia with several of the constituent seas and neighboring oceans labeled: Arafura Sea (AS), Banda Sea (BS), Celebes or Sulawesi Sea (CS), Gulf of Thailand (GT), Java Sea (JS), Indian Ocean (IO), Pacific Ocean (PO), Philippine Sea (PS), South China Sea (SCS), and Sulu Sea (SS).

Mesoscale ocean eddies are ubiquitous in the global ocean, with spatial and temporal scales on the order of 100 km and 10–100 days, respectively (Chelton et al., 2011; Kurian et al., 2011). Mesoscale ocean eddies dominate the kinetic energy signature of the ocean (e.g., Storer et al., 2022), and are generated through both barotropic and baroclinic instabilities, produced by interactions between wind, currents, and bathymetry. These eddies are dominantly nonlinear as they rotate faster than their lateral propagation, and are in approximate geostrophic and hydrostatic balance in the horizontal and vertical dimensions, respectively (e.g., Chelton et al., 2011). Important in the transport of heat, salt, nutrients, and biogeochemical tracers (e.g., Hausmann & Czaja, 2012; McGillicuddy, 2016; Melnichenko et al., 2017), eddies exhibit regional and seasonal variability in their propagation pathways, lifetimes, amplitudes, and mechanism of genesis (e.g., Halo et al., 2014; Mason et al., 2017; Zu et al., 2022).

The various deep basins and narrow tidal straits within the Maritime Continent, and their interactions with wind and currents, are crucial in generating mesoscale ocean eddies (e.g., B. Chen et al., 2020; Wang et al., 2021; Pang et al., 2022). Mesoscale ocean eddies also contribute to changes in transport along the ITF (e.g., Ismail et al., 2021; Hao et al., 2022). Eddy characteristics across the Maritime Continent vary based on basin size, sea surface temperature (SST), ocean currents, coastline distance, and bathymetry (Ffield & Gordon, 1996). Eddies in the seas of the Maritime Continent are mostly short-lived, with lifespans less than 30 days (Hao et al., 2021), and are more prevalent in the northern seas forming the inflow of the ITF (Purba et al., 2020). As a result, studies have found intraseasonal variability in surface ocean characteristics is more strongly linked to mesoscale ocean eddies, as opposed to larger-scale forcing, in the northern seas (Napitu et al., 2015).

21698996, 2025, 4, Downloaded from https://agupubs.onlinelibrary.wiley.com/doi/10.1029/2024JD042606 by University Of East Anglia, Wiley Online Library on [13/02/2025]. See the Terms and Conditions (https://onlinelibrary.wiley.com/terms-and-conditions) on Wiley Online Library for rules of use; OA articles are governed by the applicable Creative Commons License

21698996, 2025, 4, Downloaded from https://agupubs.onlinelibrary.wiley.com/doi/10.1029/2024JD042606 by University Of East Anglia, Wiley Online Library on [13/02/2025]. See the Terms and Conditions (https://onlinelibrary.wiley.com/terms-and-conditions) on Wiley Online Library for rules of use; OA articles are governed by the applicable Creative Commons License

Mesoscale ocean eddies consist of two polarities, each having characteristic features (e.g., McGillicuddy, 2016). Anticyclonic eddies are characterized by positive sea surface height anomalies (SSH) due to induced convergence through the Coriolis force, with resultant low sea level pressure (SLP) anomalies, leading to downwelling of deeper isopycnals through eddy pumping to compensate for these perturbations. Cyclonic eddies, on the other hand, have negative SSH anomalies due to Coriolis-induced divergence, with high SLP anomalies and resultant upwelling.

Signatures in SST associated with mesoscale ocean eddies act as the facilitator for interactions between these ocean features and the atmosphere (e.g., Bôas et al., 2015; Frenger et al., 2013; Gulakaram et al., 2023; J. Liu et al., 2021; Seo et al., 2023). Warm-core eddies release heat to the atmosphere through induced surface heat fluxes, which can strengthen winds and produce anomalous wind convergence. These changes can lead to enhanced instability in the atmospheric boundary layer, thereby enhancing vertical mixing, potentially leading to more cloud and rainfall. In contrast, cold-core eddies draw in heat from the atmosphere, which can weaken winds and result in anomalous wind divergence. The boundary layer is therefore more stable, with less cloud and rainfall. Both anticyclonic and cyclonic eddies can have warm and cold cores dependent on processes governing eddy vertical thermohaline structure (e.g., Y. Liu et al., 2020; W. Sun et al., 2022).

The relationship between the SST anomalies associated with eddies and influence on the atmosphere additionally results from the balance between advection and vertical mixing. When advection is weak, winds converge over the warm flank of an SST front due to the pressure gradient force (the pressure adjustment mechanism; e. g. Lindzen & Nigam, 1987; Small et al., 2008). In contrast, when advection is strong, due to enhancement of wind speed over a warm anomaly in the surface ocean, winds converge downstream (the vertical mixing mechanism; e. g. Chelton et al., 2004; Park et al., 2006; Wallace et al., 1989). These mechanisms can have competing influences on the atmospheric boundary layer (Jiang et al., 2019).

It is important to acknowledge that the background environmental state can modify the characteristics of eddies and their imprint on the atmosphere. For example, interactions with more transient processes, such as synoptic weather systems, can add additional ocean-atmosphere feedbacks (Gulakaram et al., 2023; Souza et al., 2021). Studies have also suggested seasonality in the response to, and characteristics of, eddies in regions such as the northwest Pacific, with more intense anomalies in the wintertime due to enhanced SST anomalies (X. Liu, Chang, et al., 2018; B. Sun et al., 2022). In addition, interactions between eddies and large-scale modes of variability, which regulate the environmental wind and SST field, have been observed (Roman-Stork et al., 2021).

The Maritime Continent is a region known for the modulation of atmospheric stability, convection, and rainfall by a variety of processes operating over multiple spatial and temporal scales. Processes include large-scale modes of variability, such as the Madden-Julian Oscillation (MJO, e. g. Madden & Julian, 1994), and finer-scale and more local phenomena such as the diurnal cycle of solar heating (e.g., Mori et al., 2004). Studies have also investigated the role of air-sea interactions in the Maritime Continent (see Xue et al., 2020, for a comprehensive review, primarily focusing on modeling capabilities).

Though the characteristics of eddies within the Maritime Continent are well understood, their relationship with air-sea interactions has not been studied. In fact, minimal research has been conducted into this relationship across the tropics. By using observational data to track eddies in the tropical Atlantic Ocean and analyze the associated mean atmospheric responses across the domain, Aguedjou et al. (2023) found a minimal imprint of mesoscale ocean eddies on the atmospheric boundary layer, such as in surface heat fluxes and precipitation. Toward the subtropics, such as in the South China Sea, responses in surface heat fluxes, wind, and other atmospheric properties, obtained from satellite observations, are noted in studies such as H. Liu et al. (2018). As the waters of the Maritime Continent act as an abundant heat source favoring the formation of convection, it is important to investigate if surface ocean anomalies even at the mesoscale can leave an imprint on the tropical atmosphere. Such analysis would, for example, help to inform decisions related to running coupled ocean-atmosphere models for numerical weather prediction and the complexity and/or resolution they require, by better understanding the role of the ocean, in the Maritime Continent.

In this study, we aim to identify the general properties of mesoscale ocean eddies in the Maritime Continent, and to determine if there is an atmospheric response to these eddies, which has not been analyzed in the existing literature. We use 20 years of satellite altimetry data to detect and track eddies, which are collocated in ECMWF (European Centre for Medium-Range Weather Forecasts) Reanalysis v5 (ERA5) data (Hersbach et al., 2020) to

21698996, 2025, 4, Downloaded from https://agupubs.onlinelibrary.wiley.com/doi/10.1029/2024JD042606 by University Of East Anglia, Wiley Online Library on [13/02/2025]. See the Terms and Conditions (https://onlinelibrary.wiley.com/terms-and-conditions) on Wiley Online Library for rules of use; OA articles are governed by the applicable Creative Commons License

produce composites. These composites are used to analyze whether SST anomalies at the mesoscale can interact with the atmosphere significantly enough in the Maritime Continent to affect cloud and rainfall properties, as seen in other regions. Section 2 presents the methodology used for eddy detection and tracking, construction of eddy composites for analysis of the corresponding atmospheric response, and statistical testing of the significance of these responses. We show results in Section 3, which cover the characteristics of eddies, and eddy composites in various surface and atmospheric variables. Section 4 compares these results to those obtained in previous studies, to establish hypotheses for the extent, or lack, of atmospheric responses to eddies in the Maritime Continent. Conclusions are given in Section 5.

2. Methodology

2.1. Eddy Detection and Tracking

Eddy detection is crucial for understanding eddy-induced ocean dynamics, and several methods have been developed primarily utilizing satellite altimetry data. These methods include the Okubo-Weiss parameter method (e.g., Frenger et al., 2013), where eddies are classified based on vorticity determined from the geostrophic components of velocity, and the flow and vector geometry methods (e.g., Nencioli et al., 2010), which utilize closed contours of the stream function field. The most popular method is the SSH anomaly method. This method is parameter-free, as defined eddy edges, which depend only on a single extremum, and compared to other methods, performance is better, for example, in terms of signal-to-noise ratios and avoidance of excess eddy detection (e.g., Chelton et al., 2011).

Here, we use and adapt the eddy detection and tracking algorithm, py-eddy-tracker, of Mason et al. (2014). This open-source algorithm requires SSH data input, either using sea level anomalies (SLA; deviations of the sea surface from the mean sea surface) or absolute dynamic topography (ADT; the difference between the instantaneous SSH and the marine geoid, equivalent to the sum of SLA and the mean dynamic topography). While SLA and ADT are both effective in the identification of eddies, Pegliasco et al. (2021, 2022) suggest the usage of ADT as it is more sensitive to regions with strong SSH gradients and where recurrent mesoscale features exist, or for coastal regions, and both closed and semiclosed basins, such as in the Maritime Continent. ADT is also more sensitive to tracking smaller eddies and longer trajectories, and less sensitive to detecting meanders in currents as eddies (Halo et al., 2014).

We obtained data for ADT (from here referred to just as SSH anomaly) through the Data Unification and Altimeter Combination System (DUACS; Taburet et al., 2019). DUACS is the operational multimission production system of altimeter data developed by Centre National D'Études Spatiales (CNES)/Collecte Localisation Satellites (CLS). Data products are estimated by merging along-track measurements from different altimeter missions from GEOSAT to Jason-3. These data are provided by Archiving, Validation and Interpolating of Satellite Oceanographic data (AVISO), available through the Copernicus Marine Environment Monitoring Service (CMEMS). SSH anomalies, relative to a 20-year mean, were predetermined by the data provider and available at $0.25° \times 0.25°$ horizontal grid spacing. We use 20 years of continuous daily data from December 2000 to November 2020.

The eddy detection algorithm removes a large-scale smoothed field, obtained from a Gaussian filter with a zonal (meridional) major (minor) radius of 10° (5°), from the SSH anomaly data, which accounts for their lateral propagation, visible in SSH data (Mason et al., 2014). Eddies are then identified using interpolated contours of this high-pass filtered data, calculated at intervals of 1 cm from −100 to 100 cm. Each 1 cm SSH interval is analyzed in turn, searching downward from the previously mentioned limits to 0 cm, until a closed contour is detected. From this closed contour, the algorithm employs a set number of criteria for labeling a feature as an eddy, as described in Mason et al. (2014). These criteria include constraints to the number of pixels within the final closed contour, a maximum shape error relative to an ideal fit circle, and the requirement for only one local maxima or minima within the closed contour. Once an eddy is identified, it is relabeled as the effective perimeter, with an associated effective radius, which represents the radius of a circle with the same area as that enclosed by the effective perimeter. The effective radius, hereon referred to as R, therefore equals $\sqrt{\frac{a}{\pi}}$, where a is the eddy area. Various properties are computed for each eddy, such as centroid, radius, amplitude, and area. Estimates of the along-track propagation rate were determined for each eddy using the centroids determined using the algorithm.

21698996, 2025, 4, Downloaded from https://agupubs.onlinelibrary.wiley.com/doi/10.1029/2024JD042606 by University Of East Anglia, Wiley Online Library on [13/02/2025]. See the Terms and Conditions (https://onlinelibrary.wiley.com/terms-and-conditions) on Wiley Online Library for rules of use; OA articles are governed by the applicable Creative Commons License

Pixels for SSH anomaly data, which correspond to the eddy are masked, representing regions unavailable for further eddy identification. Separation distances between centroids at times t and $t + 1$ are computed for eddy pairs of the same polarity. $t + 1$ candidates for eddies continuing the track at time t are chosen using the ellipse method as in Chelton et al. (2011). This method restricts cross-track jumping, using bounds of an ellipse with a zonally oriented major axis, 150 km radius east-west and 75 km radius north-south from the local extremum of the eddy. If multiple candidate eddies fall within an ellipse, the candidate eddy, which is a continuation of the track, is identified according to the minimum of a set of dimensionless similarity parameters (Penven et al., 2005):

$$S_{t,t+1} = \sqrt{\left(\frac{\Delta d}{d_0}\right)^2 + \left(\frac{\Delta a}{a_0}\right)^2 + \left(\frac{\Delta A}{A_0}\right)^2} \quad (1)$$

where Δd is the separation distance, Δa the difference in eddy area, and ΔA, the difference in amplitude, between eddies at times t and $t + 1$. Denominators represent characteristic values, here using those in Hao et al. (2021). A smaller value of S implies higher similarity of an eddy pair and therefore likely continued propagation of the eddy at time t. Any unused candidate eddies are labeled as new eddies. Eddy tracking continues by iteration over the time period of analysis.

2.2. Eddy Composite Construction

We use ERA5 reanalysis data (Hersbach et al., 2020) from December 2000 to November 2020 for constructing eddy composites. ERA5 is consistent with its ocean counterpart, ORAS5 (Ocean ReAnalysis System 5; Zuo et al., 2018), using both HadISST2 SST and the OSTIA sea-ice concentration to constrain surface boundary conditions. ORAS5 operates at an eddy-permitting resolution (0.25° × 0.25°) and is noted to provide an appropriate representation of the SST and sea level variability, which can be attributed, for example, to eddies in the ocean. Therefore, there is comfort in using the ERA5 data to represent the atmospheric response to these eddies, modulated by their SST anomalies. Hourly, instantaneous, and single-level ERA5 data are available at a horizontal grid spacing of 0.25° × 0.25°. For time-dependent data such as surface heat fluxes, we calculate daily means as an average of the variables over the 24 hr. Accumulated data such as precipitation and water vapor are presented as daily totals.

For each variable, a high-pass spatial filter, using a 6° × 6° Hann window, is applied, which has been used in previous studies (e.g., Aguedjou et al., 2023; Bôas et al., 2015; Delcroix et al., 2019). Application of high-pass spatial filters help to isolate signals with wavelengths larger than the extent of the window functions used, representing a larger-scale reference level. This reference can be removed from a particular variable field to produce a spatially filtered anomaly, which captures solely mesoscale variations, for example, here, in the surface and atmospheric properties analyzed. We also remove the smoothed mean annual cycle of the filtered data set derived from the first three harmonics, to produce anomalies that are both spatially and temporally filtered. To construct fitted circular composites, the eddy centroid and the radius at the mature phase, where eddy amplitude is a maximum, are taken. A two-dimensional high-resolution Cartesian grid is created for each eddy, where the eddy is normalized by its radius (R) up to $3R$. Filtered values are then interpolated to this uniform grid representing the normalized eddy. Eddies are further separated into their relevant warm-core and cold-core subgroups. To define warm-core (cold-core) eddies, the mean SST anomalies within $2/3$ of the eddy radius (Delcroix et al., 2019) must be greater than 0.1°C (less than 0.1°C). The eddies were also rotated so that the mean environmental surface wind vector is westerly (e.g., Frenger et al., 2013; J. Liu et al., 2021). Anomalies to the right of the composite centers can then be described as "downstream."

Other studies employ additional thresholds in eddy amplitude, radius at maximum amplitude, and duration, to improve the quality and robustness of results. For example, these thresholds would allow attribution of results to the strongest, largest, or longest-lasting eddies, respectively. Employing a threshold on the radius does not significantly reduce the number of eddies we analyze, compared to amplitude and duration. Using an amplitude and/or duration threshold had little impact on the spatial structure and magnitude of the anomalies we analyze (not shown), as well as reducing the number of eddies composited significantly. Therefore, we choose not to employ additional thresholds to the SST threshold when grouping and compositing eddies.

21698996, 2025, 4, Downloaded from https://agupubs.onlinelibrary.wiley.com/doi/10.1029/2024JD042606 by University Of East Anglia, Wiley Online Library on [13/02/2025]. See the Terms and Conditions (https://onlinelibrary.wiley.com/terms-and-conditions) on Wiley Online Library for rules of use; OA articles are governed by the applicable Creative Commons License

2.3. Comparison to the Environment

To determine if composite signals in anomalies associated with the identified eddies are distinguishable from the background environment, we randomly sample selected regions within our domain of analysis a number of times, roughly equivalent to the number of eddies within each labeled category of eddies for that region. See Section 3.2 for further details on the selected regions. An equivalent number of longitudes and latitudes are generated within the constraints of the region to represent eddy centroids. These random samples are composited in a similar way to the real eddies, using the mean values of eddy radii within each region, and performed for each spatiotemporally filtered variable. A *t*-test is applied for each composited set of eddies, where we chose a significance level of 5% to highlight whether a particular grid point within an eddy composite is significantly different, and therefore, distinguishable from the background environment. It should be noted that this method is sensitive to the number of eddies examined in each region, with background anomalies closer to zero, less "patchy," and more distinguishable from eddy-associated anomalies where there are more eddies (not shown).

3. Results

3.1. Eddy Characteristics

Figure 2 shows the geographical variability in eddy characteristics across the analyzed domain. There is a distinct eddy-poor belt across the equator, with approximately 150 eddies crossing a particular grid point (Figure 2a). Several regional hotspots within the tropics, particularly in the Maritime Continent, can be observed, including the Sulawesi and Sulu Seas (Figure 1), near to the inflow of the ITF, where the number of eddies per grid point is 200–300. This value is what appears to be typically observed at higher latitudes. Hotspots away from the tropics have more than 400 eddies per grid point. These areas include seas near Japan, extending eastward into the northwest Pacific Ocean, within the Kuroshio Extension.

Eddies across the tropics have smaller mean peak amplitudes in their SSH anomalies (approximately 2 cm), reaching up to 4 cm in the previously mentioned hotspots within the Maritime Continent (Figure 2b). These peaks are much lower than in subtropical eddy-rich regions such as the Bay of Bengal and South China Sea, where amplitudes can be up to and above 10 cm. Even more striking is the mean amplitude exceeding 10 cm in most of the northwest Pacific, primarily east of Japan toward the central northern Pacific, as well as toward Kamchatka and the South China Sea.

There is a distinct latitudinal gradient in the mean radius of eddies (Figure 2c). Across the open ocean, mean radii in the tropics are between 110 and 130 km, going down to around 50–70 km toward the extratropics. Within the seas of the Maritime Continent, mean radii of eddies are smaller than in the tropical open ocean, up to 80 km in the internal seas, and much lower near the coastlines.

Mean eddy duration largely follows the distribution of the number of eddies, where eddies in the tropics are short-lived with maxima of 10 days (Figure 2d). Regional eddy hotspots have slightly longer lifetimes, up to 15 days in the northeastern seas of the Maritime Continent, and up to 20 days toward the southeast tropical Indian Ocean. These values are smaller than values of up to 40–50 days in regions such as the Bay of Bengal. These eddies are also much more short-lived than those in the extratropics where lifetimes reach above 50 days in the open ocean. In the northwestern Pacific, bands of shorter lifetimes, one located around 35°N and another extending from Kamchatka southward past Japan toward Taiwan, are observed. Here, eddies have lifetimes of maximum 20 days.

Eddies in the tropics, particularly in the open ocean, have greater mean propagation rates, up to around 25 km day^{-1} (Figure 2e). Within the internal seas of the Maritime Continent, propagation rates reduce to around 15–20 km day^{-1}. Tending toward higher latitudes, mean propagation rates are much lower, around 5–10 km day^{-1}.

3.2. Eddy Characteristics: Regional Comparison

We focus our study on three regions in the Maritime Continent. These regions are shown as the southern three polygons in Figure 2f, with their spatial extents chosen for consistency with existing literature. From south to north, these are the southeast tropical Indian Ocean (e.g., Ismail et al., 2021; Wang et al., 2021; Yang et al., 2015; Zu et al., 2022), hereon referred to as the SETIO, the Sulawesi Sea (e.g., Hao et al., 2021, 2022), and the South

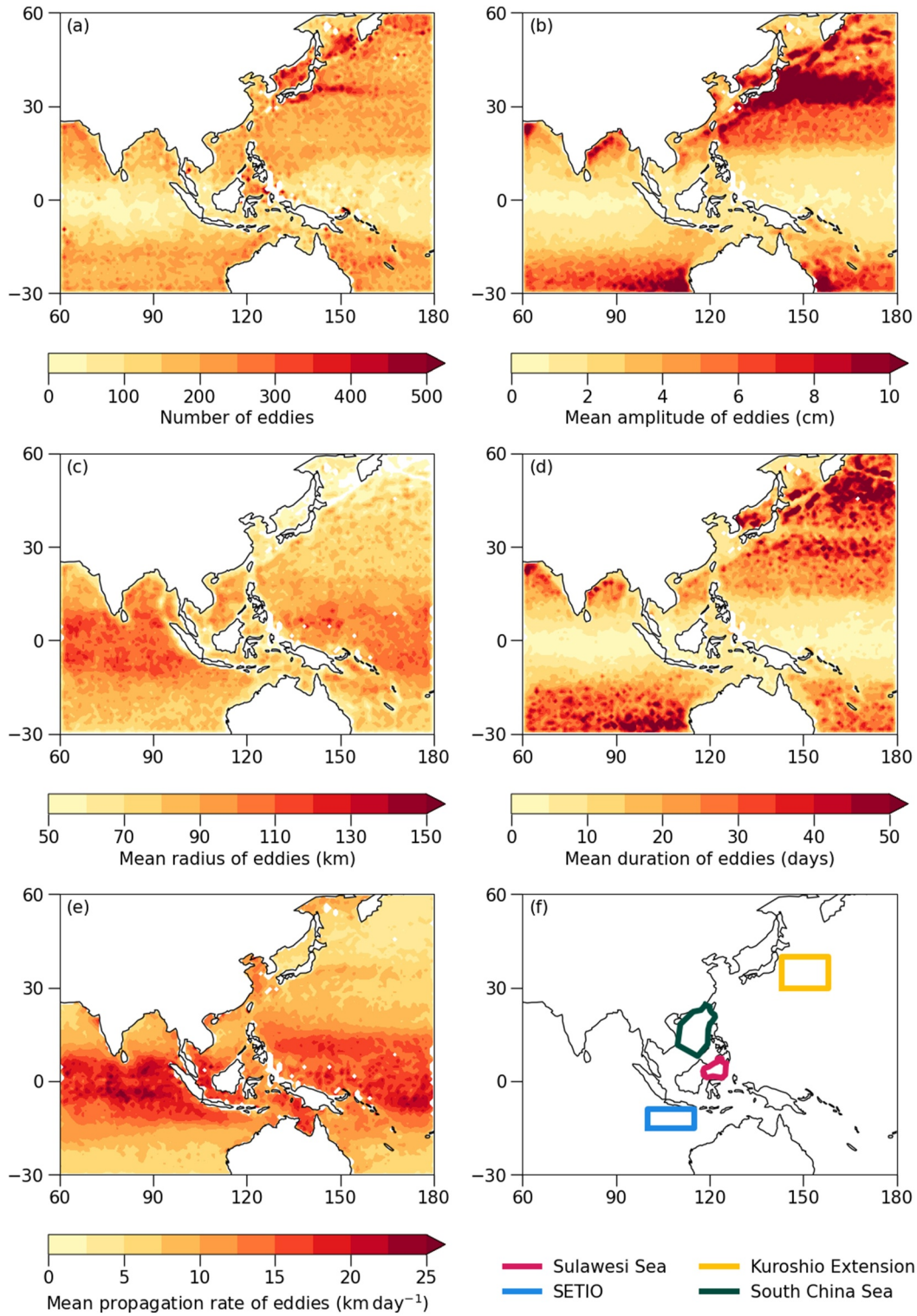

Figure 2. (a) Distribution of the number of eddies identified from December 2000 to November 2020, where sums are calculated within bins of 1° × 1°. The other four panels represent the mean amplitude (b), radius (c), duration (d), and propagation rate (e) of all eddies. Values in panels (b)–(d) are calculated from sums of eddy properties when each eddy is at peak amplitude, whereas the propagation rate (e) is calculated along track and plotted where eddy is at peak amplitude. Panel (f) highlights the Kuroshio Extension (yellow), South China Sea (green), Sulawesi Sea (pink), and southeast tropical Indian Ocean (SETIO; blue) from north to south respectively, which are the regions used in later analysis.

21698996, 2025, 4, Downloaded from https://agupubs.onlinelibrary.wiley.com/doi/10.1029/2024JD042606 by University Of East Anglia, Wiley Online Library on [13/02/2025]. See the Terms and Conditions (https://onlinelibrary.wiley.com/terms-and-conditions) on Wiley Online Library for rules of use; OA articles are governed by the applicable Creative Commons License

Table 1
The Number of Anticyclonic and Cyclonic Eddies Identified in Each Region

	Anticyclonic eddies	Cyclonic eddies
Kuroshio Extension	16,456 (14,137 = 85.9%)	16,192 (13,653 = 84.3%)
South China Sea	10,476 (5,934 = 56.6%)	10,335 (5,832 = 56.4%)
Southeast tropical Indian Ocean	8,638 (3,716 = 43.0%)	8,261 (3,605 = 43.6%)
Sulawesi Sea	4,382 (2,121 = 48.4%)	3,224 (1,621 = 50.3%)

Note. Values in brackets represent the number of eddies used for later composites after imposing an absolute threshold of 0.1°C on the core of the eddy. This value is also presented as a percentage of the total number of eddies for each polarity.

China Sea (e.g., He et al., 2018; H. Liu et al., 2018; Y. Liu et al., 2020). Eddies were associated with a particular region if they reach peak amplitude when their centroid is within the respective spatial bounds of each region. All three regions are known for the generation of mesoscale ocean eddies, primarily through the interaction of ocean currents and resultant changes to water properties.

However, the South China Sea is the only region in the Maritime Continent, which has been studied, with regards to air-sea interactions associated with eddies. Therefore, we also choose a well-known extratropical region, the Kuroshio Extension, within the northwest Pacific, to facilitate a comparison with existing studies. The Kuroshio Extension is an environment rich in high amplitude eddies, produced by ocean currents, which interact to form a strong meridional SST gradient (e.g., Chelton et al., 2011; Cheng et al., 2014). Studies within the Kuroshio Extension have investigated the signatures of eddies at the surface and depth (W. Sun et al., 2022), in addition to surface heat flux anomalies and impacts on the atmospheric boundary layer (Ma et al., 2015, 2016). A comparison of this region with those in the Maritime Continent allows testing and validation of the existing methodology, and provides reassurance that the approach taken is suitable.

Table 1 shows the number of eddies identified in each of the four regions. A sharp reduction in the number of eddies is noted, as observed in Figure 2a, from the extratropics in the Kuroshio Extension (a total of 32648), to near-equatorial regions such as the Sulawesi (a total of 7,606). Histograms showing the distribution of mean amplitudes, radii, duration, and propagation rates of tracked eddies in the selected regions are provided in Figure 3. Here, we separate eddies into anticyclonic and cyclonic eddies.

The mean amplitude of eddies in the Sulawesi Sea and SETIO are similar, around 2.5 cm for anticyclonic eddies (Figure 3a) and 3 cm for cyclonic eddies (Figure 3b). Eddies in the South China Sea are around 1–1.5 cm stronger than those in the other two Maritime Continent regions. Kuroshio Extension eddies are much stronger, over 5 times that of eddies in the Sulawesi Sea and SETIO. In all three regions other than the South China Sea, cyclonic eddies have greater amplitude than anticyclonic eddies.

The mean radius associated with eddies in the Sulawesi Sea and Kuroshio Extension is similar (70–80 km) for both anticyclonic eddies (Figure 3c) and cyclonic eddies (Figure 3d). South China Sea eddies are greater in size, around 83 km in radius, though SETIO eddies are the largest out of the four regions, with radii above 90 km. Cyclonic eddies are greater in size than anticyclonic eddies in the Sulawesi Sea and SETIO, whereas the two eddy types are similar in size in the South China Sea and Kuroshio Extension.

Sulawesi Sea eddies are the most short-lived, lasting around 9–10 days (Figures 3e and 3f). South China Sea anticyclonic eddies (cyclonic eddies) last for 4 days longer (2 days less) than those in the SETIO, but both sets of eddies last for twice as long as Sulawesi Sea eddies. In contrast, Kuroshio Extension eddies can last for between 3 and 4 weeks. South China Sea and Sulawesi anticyclonic eddies last longer than their respective cyclonic eddies, and the opposite is observed for the other two regions.

There is similarity between the mean propagation rates of anticyclonic eddies (Figure 3g) and cyclonic eddies (Figure 3h) in each region, with differences of only up to around 1 km day^{-1}. SETIO eddies propagate the fastest, with means up to around 15 km day^{-1}. These rates are up to 4 km day^{-1} greater than those in the Sulawesi Sea, but almost double the propagation rates observed in the South China Sea and Kuroshio Extension.

21698996, 2025, 4, Downloaded from https://agupubs.onlinelibrary.wiley.com/doi/10.1029/2024JD042606 by University Of East Anglia, Wiley Online Library on [13/02/2025]. See the Terms and Conditions (https://onlinelibrary.wiley.com/terms-and-conditions) on Wiley Online Library for rules of use; OA articles are governed by the applicable Creative Commons License

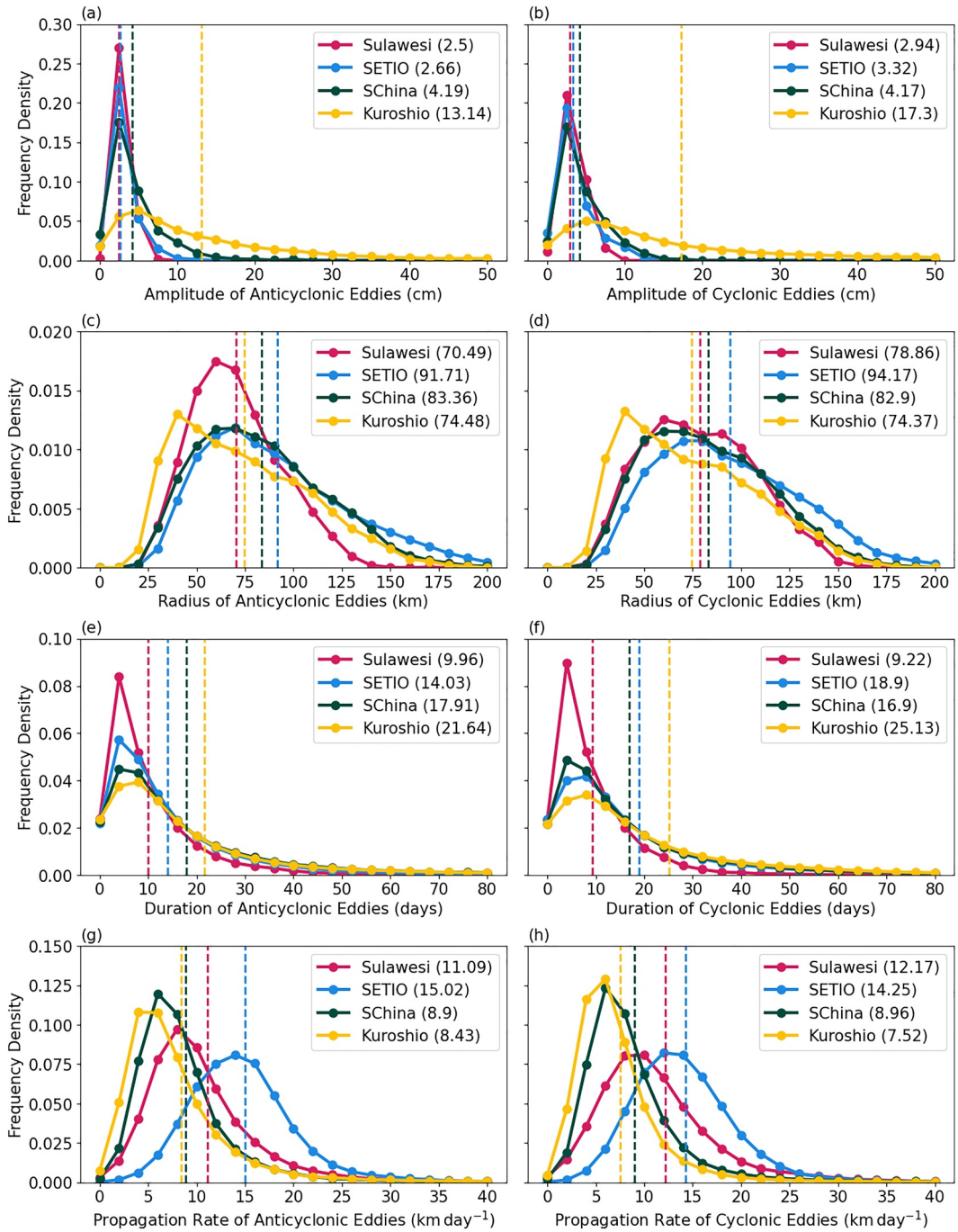

Figure 3. Histograms of the amplitude (a–b), radius (c–d), duration (e–f), and propagation rate (g–h) of anticyclonic and cyclonic eddies, respectively, identified in the studied eddy hotspots. The Sulawesi Sea, southeast tropical Indian Ocean (SETIO), South China Sea, and Kuroshio Extension are marked by pink, blue, green, and yellow colors, respectively. Dashed vertical lines mark the mean of each variable for the eddies in each region, as indicated in the legend. Upper limits for each variable on the *x*-axis are chosen to aid visual clarity.

3.3. Eddy Composites

Here, we present composites of the property anomalies associated with mesoscale ocean eddies in each of the hotspot regions (Figures 4–7) in order to identify possible spatial patterns. We analyze interactions at the air-sea interface associated with eddies using sensible and latent heat fluxes (SHF and LHF, respectively) and wind

21698996, 2025, 4, Downloaded from https://agupubs.onlinelibrary.wiley.com/doi/10.1029/2024JD042606 by University Of East Anglia, Wiley Online Library on [13/02/2025]. See the Terms and Conditions (https://onlinelibrary.wiley.com/terms-and-conditions) on Wiley Online Library for rules of use; OA articles are governed by the applicable Creative Commons License

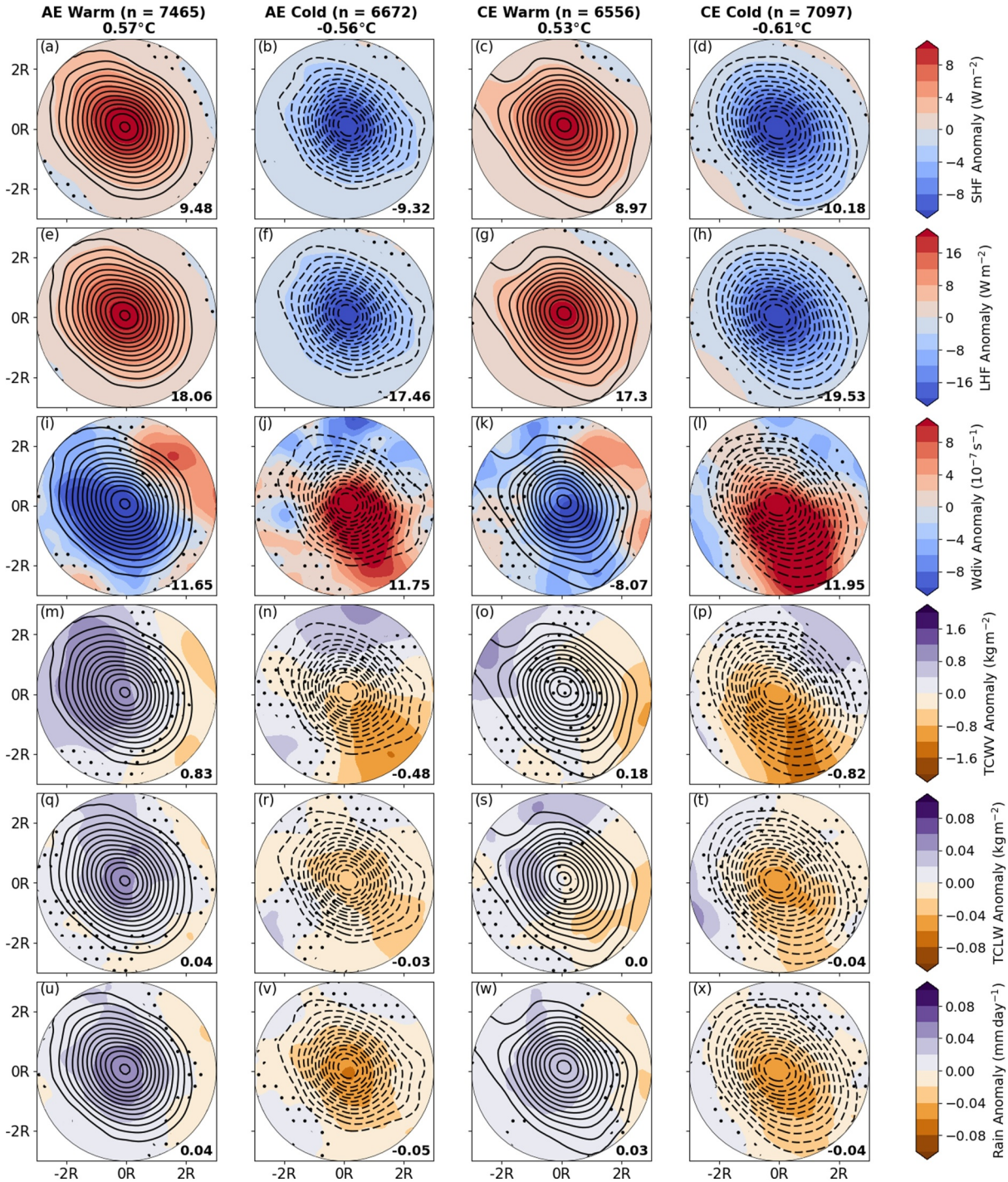

Figure 4. (a–d) Eddy composites of surface sensible heat flux anomalies, shown in filled contours, for the four categories of eddies (anticyclonic warm, anticyclonic cold, cyclonic warm, and cyclonic cold, respectively) in the Kuroshio Extension, plotted up to 3*R* from the centroid. Contours represent sea surface temperature anomalies in increments (reductions) of 0.05°C, starting from 0.1°C (−0.1°C) for warm (cold) eddies. Values of *n* indicate the number of eddies composited within each panel. "Eddy-averaged" (averaged up to 1*R*) anomalies in sea surface temperature are provided next to these. (e–h), (i–l), (m–p), (q–t), and (u–x) are the same as (a–d), except filled contours now represent surface latent heat flux, 10-m wind divergence, total column water vapor, total cloud liquid water, and rain anomalies, respectively. The values in the bottom right of each panel represent "eddy-averaged" values for each property. Dots represent regions where there is no significant difference between the eddy composites and the background environment, using a *t*-test at the 5% significance level, as described in Section 2.3.

21698996, 2025, 4, Downloaded from https://agupubs.onlinelibrary.wiley.com/doi/10.1029/2024JD042606 by University Of East Anglia, Wiley Online Library on [13/02/2025]. See the Terms and Conditions (https://onlinelibrary.wiley.com/terms-and-conditions) on Wiley Online Library for rules of use; OA articles are governed by the applicable Creative Commons License

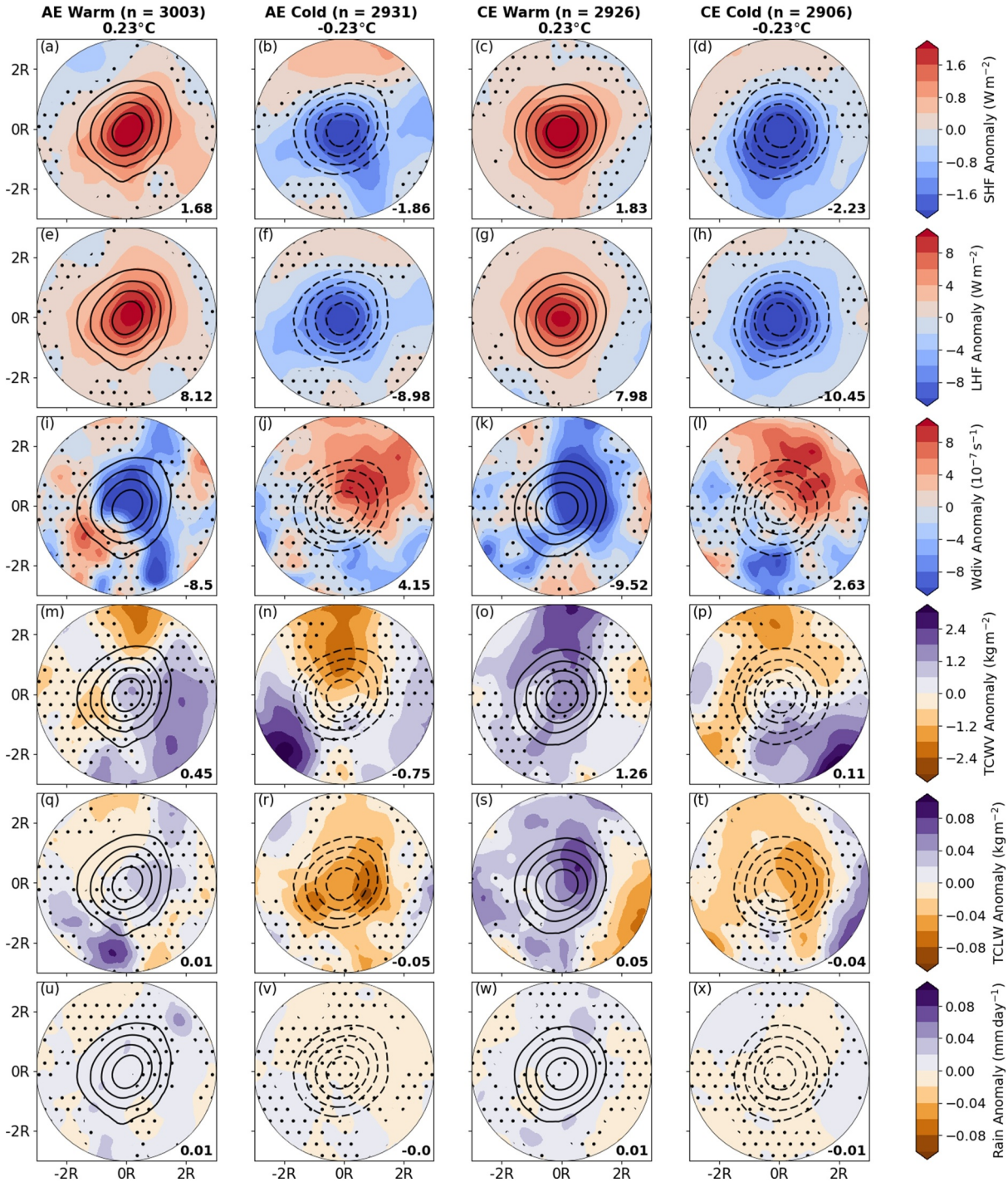

Figure 5. (a–d) Eddy composites of surface sensible heat flux anomalies, shown in filled contours, for the four categories of eddies (anticyclonic warm, anticyclonic cold, cyclonic warm, and cyclonic cold, respectively) in the South China Sea, plotted up to 3*R* from the centroid. Contours represent sea surface temperature anomalies in increments (reductions) of 0.05°C, starting from 0.1°C (−0.1°C) for warm (cold) eddies. Values of *n* indicate the number of eddies composited within each panel. "Eddy-averaged" (averaged up to 1*R*) anomalies in sea surface temperature are provided next to these. (e–h), (i–l), (m–p), (q–t), and (u–x) are the same as (a–d), except filled contours now represent surface latent heat flux, 10-m wind divergence, total column water vapor, total cloud liquid water, and rain anomalies, respectively. The values in the bottom right of each panel represent "eddy-averaged" values for each property. Dots represent regions where there is no significant difference between the eddy composites and the background environment, using a *t*-test at the 5% significance level, as described in Section 2.3. Note that, compared to Figure 4, the color scales for surface heat flux and total cloud liquid water anomalies have been changed for better visualization of results between the three regions of the Maritime Continent.

21698996, 2025, 4, Downloaded from https://agupubs.onlinelibrary.wiley.com/doi/10.1029/2024JD042606 by University Of East Anglia, Wiley Online Library on [13/02/2025]. See the Terms and Conditions (https://onlinelibrary.wiley.com/terms-and-conditions) on Wiley Online Library for rules of use; OA articles are governed by the applicable Creative Commons License

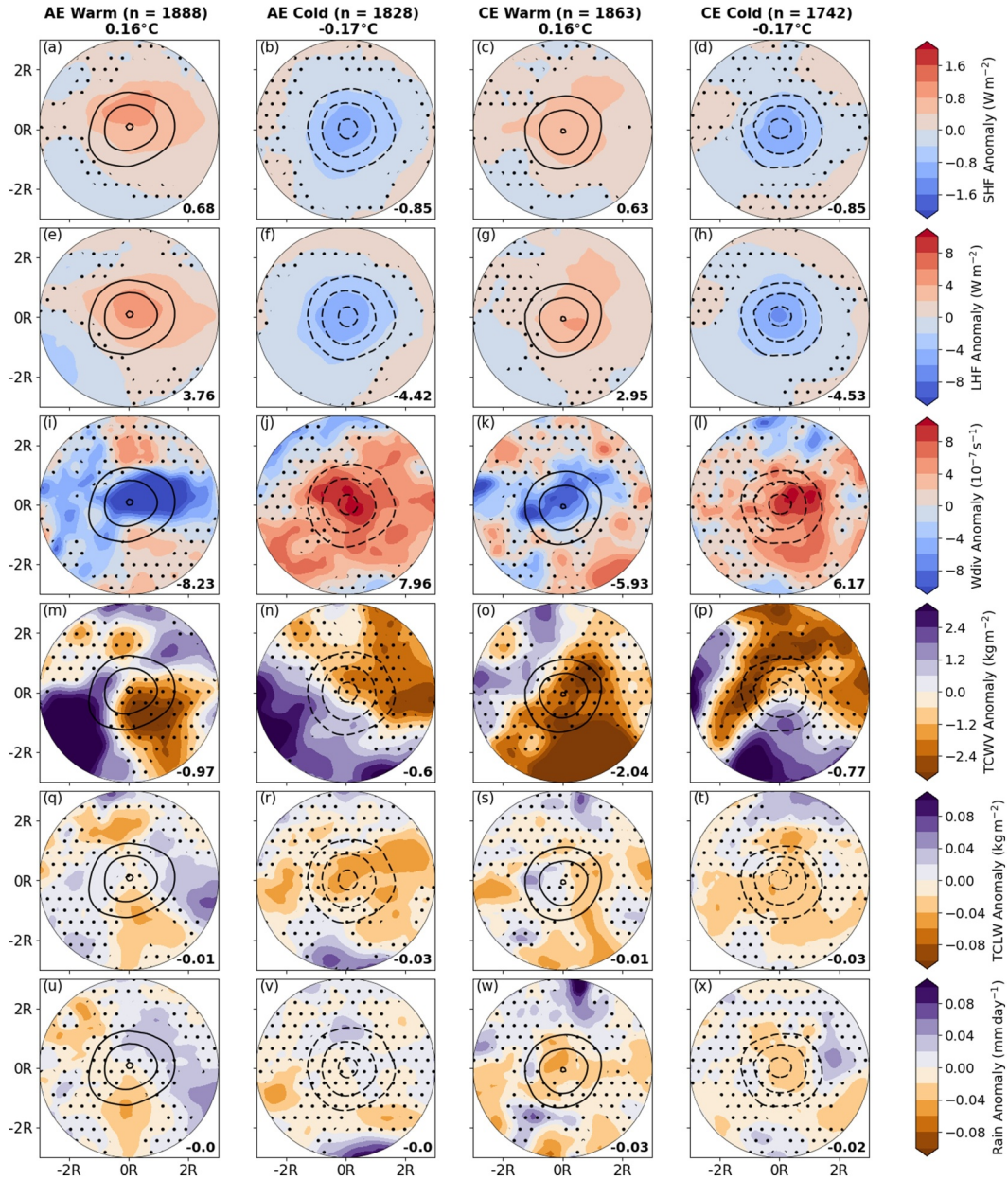

Figure 6. (a–d) Eddy composites of surface sensible heat flux anomalies, shown in filled contours, for the four categories of eddies (anticyclonic warm, anticyclonic cold, cyclonic warm, and cyclonic cold, respectively) in the southeast tropical Indian Ocean, plotted up to 3*R* from the centroid. Contours represent sea surface temperature anomalies in increments (reductions) of 0.05°C, starting from 0.1°C (−0.1°C) for warm (cold) eddies. Values of *n* indicate the number of eddies composited within each panel. "Eddy-averaged" (averaged up to 1*R*) anomalies in sea surface temperature are provided next to these. (e–h), (i–l), (m–p), (q–t), and (u–x) are the same as (a–d), except filled contours now represent surface latent heat flux, 10-m wind divergence, total column water vapor, total cloud liquid water, and rain anomalies, respectively. The values in the bottom right of each panel represent "eddy-averaged" values for each property. Dots represent regions where there is no significant difference between the eddy composites and the background environment, using a *t*-test at the 5% significance level, as described in Section 2.3. Note that, compared to Figure 4, the color scales for surface heat flux and total cloud liquid water anomalies have been changed for better visualization of results between the three regions of the Maritime Continent.

divergence at 10 m. Total column water vapor (TCWV), cloud liquid water (TCLW), and rainfall are also plotted for understanding changes to atmospheric moisture and cloud presence, which may be linked to the induced air-sea interactions. Note that color scales for the three Maritime Continent regions (Figures 5–7) differ for some

21698996, 2025, 4, Downloaded from https://agupubs.onlinelibrary.wiley.com/doi/10.1029/2024JD042606 by University Of East Anglia, Wiley Online Library on [13/02/2025]. See the Terms and Conditions (https://onlinelibrary.wiley.com/terms-and-conditions) on Wiley Online Library for rules of use; OA articles are governed by the applicable Creative Commons License

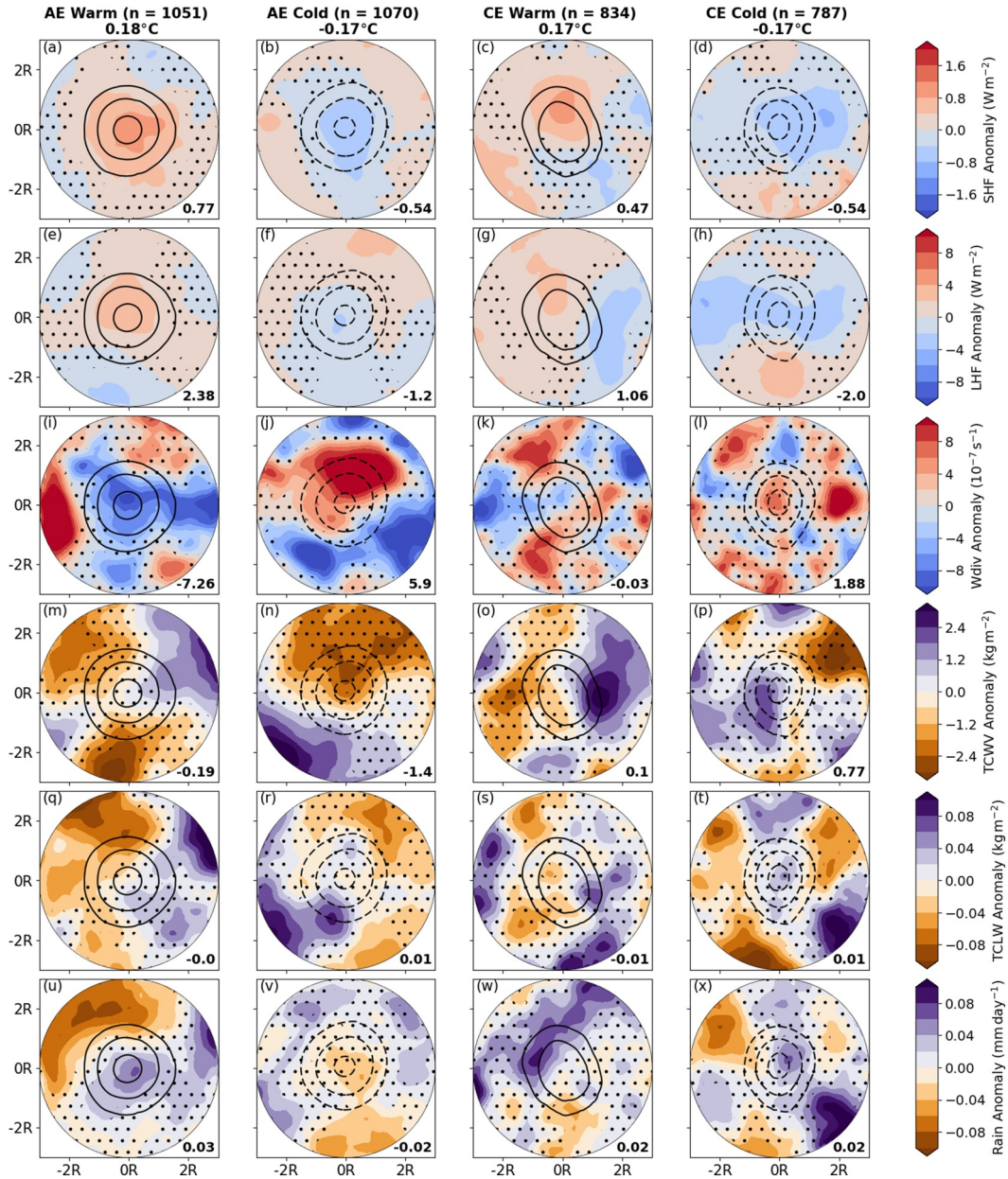

Figure 7. (a–d) Eddy composites of surface sensible heat flux anomalies, shown in filled contours, for the four categories of eddies (anticyclonic warm, anticyclonic cold, cyclonic warm, and cyclonic cold, respectively) in the Sulawesi Sea, plotted up to 3*R* from the centroid. Contours represent sea surface temperature anomalies in increments (reductions) of 0.05°C, starting from 0.1°C (−0.1°C) for warm (cold) eddies. Values of *n* indicate the number of eddies composited within each panel. "Eddy-averaged" (averaged up to 1*R*) anomalies in sea surface temperature are provided next to these. (e–h), (i–l), (m–p), (q–t), and (u–x) are the same as (a–d), except filled contours now represent surface latent heat flux, 10-m wind divergence, total column water vapor, total cloud liquid water, and rain anomalies, respectively. The values in the bottom right of each panel represent "eddy-averaged" values for each property. Dots represent regions where there is no significant difference between the eddy composites and the background environment, using a *t*-test at the 5% significance level, as described in Section 2.3. Note that, compared to Figure 4, the color scales for surface heat flux and total cloud liquid water anomalies have been changed for better visualization of results between the three regions of the Maritime Continent.

variables compared to the Kuroshio Extension (Figure 4) to better visualize results and to account for geographical variability in the responses. Any eddies with absolute SST anomalies below 0.1°C, as outlined in the methodology, were discarded. The total number of eddies therefore used in these composites is shown in brackets in Table 1.

21698996, 2025, 4, Downloaded from https://agupubs.onlinelibrary.wiley.com/doi/10.1029/2024JD042606 by University Of East Anglia, Wiley Online Library on [13/02/2025]. See the Terms and Conditions (https://onlinelibrary.wiley.com/terms-and-conditions) on Wiley Online Library for rules of use; OA articles are governed by the applicable Creative Commons License

21698996, 2025, 4, Downloaded from https://agupubs.onlinelibrary.wiley.com/doi/10.1029/2024JD042606 by University Of East Anglia, Wiley Online Library on [13/02/2025]. See the Terms and Conditions (https://onlinelibrary.wiley.com/terms-and-conditions) on Wiley Online Library for rules of use; OA articles are governed by the applicable Creative Commons License

3.3.1. Region 1: Kuroshio Extension (The Extratropics)

Absolute eddy-averaged SST anomalies in the Kuroshio Extension region are around 0.6°C across the four eddy types analyzed, with anomalies extending to beyond 2*R* (Figure 4). There is strong correspondence between SST and SHF anomalies in the Kuroshio Extension, where absolute eddy-averaged anomalies can reach values around 10 W m^{-2} (Figures 4a–4d). These anomalies are significantly different from the background environment. Similar correspondence can be observed between SST and LHF anomalies (Figures 4e–4h). Eddy-averaged LHF anomalies are nearly double the SHF anomalies and are similarly significant compared to the background environment. The sign of both surface heat flux anomalies extend over 2R, with fluxes out of (into) the ocean for warm-core (cold-core) eddies.

There is also a degree of correspondence between SST anomalies and centers of wind divergence anomalies (Figures 4i–4l). Anomalous convergence (divergence) is observed over warm (cold) eddies, with these anomalies also noted downstream. Absolute eddy-averaged anomalies are around 10^{-6} s^{-1}, and are also significantly different from the background environment.

Changes to TCWV anomalies have similar spatial structure to the wind divergence anomalies, aside from warm cyclonic eddies (Figures 4m–4p). Generally, warm-core (cold-core) eddies have increases (decreases) in TCWV near to centers of surface convergence (divergence), which are off-center relative to the SST anomaly. Absolute eddy-averaged anomalies are up to around 1 kg m^{-2}, while values corresponding to regions with pronounced wind divergence anomalies approach 2 kg m^{-2}. TCWV anomalies are significant relative to the background environment. TCLW anomalies tend to follow the spatial distribution as seen with TCWV, where increases (decreases) in TCLW by up to 0.05 kg m^{-2} occur relative to warm-core (cold-core) eddies (Figures 4q–4t). The signal of these anomalies relative to TCWV, however, is slightly weaker.

Rain anomalies over Kuroshio Extension eddies have absolute eddy-averaged values around 0.05 mm day^{-1}, reaching up to 0.1 mm day^{-1} within the center of the composites (Figures 4u–4x). There is strong spatial coherence between the SST anomalies associated with the eddies and the rain anomalies, with increases (reductions) in rain over warm (cold) eddies. These anomalies are significant relative to the background environment.

3.3.2. Region 2: South China Sea (Northern Maritime Continent)

SST anomalies associated with eddies in the South China Sea are between 0.2 and 0.25°C, and extend to 1.5–2*R* (Figure 5). Eddy-averaged SHF anomalies within the South China Sea are not as strong as those in the Kuroshio Extension—around 2 W m^{-2}—but are spatially coherent with the SST anomalies and significantly different from the background environment (Figures 5a–5d). Spatial coherence and significance is also the case for LHF anomalies, where absolute eddy-averaged values are up to around 10 W m^{-2} (Figures 5e–5h). Heat fluxes out of (into) the ocean are associated with warm-core (cold-core) eddies.

In this region, wind divergence anomaly centers are located downstream of eddies (Figures 5i–5l). Downstream convergence (divergence) is associated with warm (cold) eddies in the rotated composites. Absolute anomalies are slightly weaker than in the Kuroshio Extension, being just shy of 10^{-6} s^{-1}. Nonetheless, these anomalies are statistically significant relative to the background environment.

The distribution of TCWV anomalies (Figures 5m–5p) roughly follow that of wind divergence. Enhancements (reductions) in TCWV of just over 1 kg m^{-2}, related to centers of surface convergence (divergence), are associated with warm-core (cold-core) eddies. It must be noted that these anomalies are not as spatially coherent with respect to the SST anomaly itself, though the anomalies are significant. The robustness of the signal in TCLW is of similar strength (Figures 5q–5t). Peaks in absolute TCLW anomalies are around 0.05 kg m^{-2} at the center, though are not as robust for warm anticyclonic eddies (Figure 5q).

Rain anomalies are generally not statistically significant relative to the background environment (Figures 5u–5x). Eddies in the South China Sea have near-zero eddy-averaged rain values, with no observable signal related to the eddy. However, they do get the correct sign in cases where warm-core and cold-core eddies have anomalies 0.1 mm day^{-1} and −0.1 mm day^{-1}, respectively.

21698996, 2025, 4, Downloaded from https://agupubs.onlinelibrary.wiley.com/doi/10.1029/2024JD042606 by University Of East Anglia, Wiley Online Library on [13/02/2025]. See the Terms and Conditions (https://onlinelibrary.wiley.com/terms-and-conditions) on Wiley Online Library for rules of use; OA articles are governed by the applicable Creative Commons License

3.3.3. Region 3: Southeast Tropical Indian Ocean (Southern Maritime Continent)

Eddy-related SST anomalies in the SETIO are just over 0.15°C, with spatial extents confined to around 1*R* (Figure 6). Absolute eddy-averaged SHF anomalies are weaker than in the South China Sea, between 0.6 and 0.9 W m^{-2} (Figures 6a–6d). However, there remains spatial correspondence with SST anomalies, and SHF anomalies are significant relative to the background environment. Absolute eddy-averaged LHF anomalies are around 5 times greater than that the SHF anomalies (Figures 6e–6h). Anomalies in LHF are also significant from the background environment. As in the previous two regions, heat fluxes are observed coming out of (into) the ocean for warm-core (cold-core) eddies.

Anomalous convergence (divergence) is associated with the warm-core (cold-core) eddies in the SETIO (Figures 6i–6l). The magnitude of these anomalies are similar to those in the South China Sea, though there remains spatial coherence with the SST anomalies, particularly for the cyclonic eddies (Figures 6k and 6l). In comparison, the anticyclonic eddies have responses both over the eddy center and downstream (Figures 6i and 6j). Wind divergence anomalies in all eddy categories are significant relative to the background environment.

Despite the anomalies seen in SHF, LHF, and wind divergence, TCWV anomalies do not appear to have a coherent spatial structure relative to the SST anomalies (Figures 6m–6p). Absolute TCWV anomalies around the composite exceed 3 kg m^{-2}, and are only significant relative to the background environment where anomalies reach these magnitudes. Similar spatial incoherence is attributed to the TCLW anomalies (Figures 6q–6t). While negative TCLW anomalies (eddy-averaged means of −0.03 kg m^{-2}) are associated with cold eddies (Figures 6r and 6t), which show coherence with the wind divergence anomalies (Figures 6j and 6l), there is not as strong an association as that seen for example, in the Kuroshio Extension and the South China Sea.

While eddy-averaged rain anomalies are greater than those in the South China Sea, responses in the SETIO show little direct association with the SST anomaly, contrasting the other variables (Figures 6u–6x). Centers of positive and negative sign, significant from the background environment, are dotted around the composites. Only cold cyclonic eddies have a slightly similar response to that observed in the Kuroshio Extension (Figure 4).

3.3.4. Region 4: Sulawesi Sea (Near-Equatorial Maritime Continent)

Absolute SST anomalies associated with eddies in the Sulawesi Sea are similar to those in the SETIO, extending to 1–1.5*R* (Figure 7). Mean eddy-averaged SHF anomalies are weak, with absolute eddy-averaged values ranging between 0.5 and 0.8 W m^{-2} (Figures 7a–7d). LHF anomalies are around 2–3 times the magnitude of the SHF anomalies (Figures 7e–7h). While both anomalies are statistically significant, the responses are not as centered over the SST anomaly as in the SETIO, aside from the anticyclonic eddies (Figures 7a–7b and 7e–7f). Nevertheless, the eddy-averaged signal is suggestive of heat fluxes coming out of (into) the ocean for warm-core (cold-core) eddies.

Anomalies in wind divergence show less spatial coherence with the SST anomalies, as in the SETIO (Figures 7i–7l). Anticyclonic eddies have divergence (convergence) centered slightly over the warm-core (cold-core) eddies, but this is not the case for the cyclonic eddies where the signal is weaker and patchier. Therefore, the association between the eddies, their SST anomalies, and wind divergence is fairly weak, even if individual anomaly centers are significant from the background environment.

As in the SETIO, there is no visible coherence between eddy SST anomalies and anomalies in TCWV (Figures 7m–7p). There is generally a random distribution of centers of either strongly negative and positive TCWV anomalies of absolute values up to 3 kg m^{-2}. Only cold anticyclonic eddies show coherence with existing observations, where anomalies of surface divergence (Figure 7j) appear to correspond to negative TCWV anomalies at the center of the eddy (Figure 7n). The anomalies vary in statistical significance, and these results are similar to what is observed for TCLW (Figures 7q–7t), where the signal, while largely paralleling that of TCWV, appears to be patchier.

Rain anomalies also have little correspondence with the eddy SST anomalies (Figures 7u–7x). While the absolute eddy-averaged values are stronger than the SETIO and South China Sea, at a maximum of 0.03 mm day^{-1}, the signal is also patchy, where anomaly centers dotted around the composites remain significant from the background environment. These anomalies can exceed absolute values of 0.1 mm day^{-1}. An exception would be the anticyclonic eddies, where slightly positive and negative anomalies are located over the centers of the warm-core

21698996, 2025, 4, Downloaded from https://agupubs.onlinelibrary.wiley.com/doi/10.1029/2024JD042606 by University Of East Anglia, Wiley Online Library on [13/02/2025]. See the Terms and Conditions (https://onlinelibrary.wiley.com/terms-and-conditions) on Wiley Online Library for rules of use; OA articles are governed by the applicable Creative Commons License

and cold-core eddies, respectively (Figures 7u and 7v). This response, however, remains less robust than that in the Kuroshio Extension (Figure 4).

4. Discussion

In Section 3.1, we identified a belt of short-lived, and low in number, eddies across the equator, while eddies were more prevalent and longer-lived at higher latitudes (Figure 2). Eddies are much smaller at higher latitudes as expected from the Rossby radius of deformation. However, eddies in the internal seas of the Maritime Continent are also smaller than other near-equatorial regions. The duration and distribution of these eddies had spatial similarity to the peak amplitude of identified eddies. The speed of eddy propagation also showed latitudinal dependency. These results were even more apparent when analyzing the eddy characteristics through regional distributions and means (Figure 3).

The properties and distribution patterns of eddies we show here agree with previous studies, including those for the Kuroshio Extension and extratropics (e.g., Chelton et al., 2011; Cheng et al., 2014) and across the Maritime Continent (e.g., Hao et al., 2021; Ismail et al., 2021; Wang et al., 2021). Propagation speed has been noted to decrease with latitude, with speeds similar to those of Rossby waves closer to the tropics (G. Chen et al., 2022; Ni et al., 2020). Such faster propagation speed at lower latitudes may make it harder to detect eddies, leading to a visibly eddy-poor tropics (Fu et al., 2010). Chelton et al. (2007), on the other hand, suggest that most of the energy propagation in the tropics is presented as Rossby waves instead of mesoscale ocean eddies. In the Maritime Continent, however, the fewer number of eddies in many of the internal basins is largely due to shallow bathymetry, preventing the existence of mesoscale ocean eddies in the first instance.

It is important to highlight that data resolution may be a barrier in fully characterizing eddies within the internal seas of the Maritime Continent, due to complex regional geography, which may not be fully resolved with the employed data set. Nonetheless, the employed SSH data set, widely used in studies at the mesoscale, remains the highest horizontal resolution data available for such an extensive time period of analysis.

The Kuroshio Extension is shown to have eddy-averaged absolute SST anomalies of around 0.6°C (Figure 4). These SST anomalies have strong spatial correspondence with surface heat fluxes (absolute values of around 10 W m^{-2} and 20 W m^{-2} for SHF and LHF, respectively) and wind divergence. These results are statistically significant relative to the background environment. Patterns in wind divergence anomalies in the Kuroshio Extension could favor either the pressure adjustment mechanism (Lindzen & Nigam, 1987) or the vertical mixing mechanism (Wallace et al., 1989), as anomalies in divergence are centered dominantly over the eddy or just downstream.

We also observe significant TCWV and TCLW anomalies, which correspond roughly to the spatial signature in wind divergence. Spatially coherent rain anomalies averaging to absolute values of around 0.05 mm day^{-1} are of similar magnitude to that observed in previously cited literature (e.g., Ma et al., 2015, 2016). Given our results for the Kuroshio Extension are consistent with the literature, there is confidence in applying this methodology to the remaining areas.

The statistical significance and magnitude of anomalies vary in the Maritime Continent, however. Eddies in the South China Sea exhibit absolute eddy-averaged SST anomalies of nearly 0.25°C, and anomalies of around 2 W m^{-2} and 10 W m^{-2} for SHF and LHF, respectively, statistically significant relative to the background environment (Figure 5). Similarly, significant wind divergence anomalies just downstream of the eddies were observed. Eddy-averaged anomalies in TCWV and TCLW are similar to the Kuroshio Extension. Rain anomalies, while being of the correct sign over the eddy itself, are near-zero. These results are consistent with that of H. Liu et al. (2018), where a potential response in column water vapor is observed, but not so strongly in precipitation.

The other two regions of the Maritime Continent—the SETIO (Figure 6) and Sulawesi Sea (Figure 7)—show weaker SST anomalies (just over 0.15°C), along with weaker absolute eddy-averaged SHF (0.5–1 W m^{-2}) and LHF anomalies (3–4.5 W m^{-2} and 1–2.5 W m^{-2} for the two regions, respectively). Wind divergence anomalies differ between the SETIO and Sulawesi Sea eddies, with a signal over and downstream of the eddies in the SETIO, but a slightly less robust response in the Sulawesi Sea. All anomalies remain statistically significant relative to the background environment. However, TCWV, TCLW, and rain anomalies are also fairly patchy in each region. No coherent signal can be directly attributed to the eddies, even though

21698996, 2025, 4, Downloaded from https://agupubs.onlinelibrary.wiley.com/doi/10.1029/2024JD042606 by University Of East Anglia, Wiley Online Library on [13/02/2025]. See the Terms and Conditions (https://onlinelibrary.wiley.com/terms-and-conditions) on Wiley Online Library for rules of use; OA articles are governed by the applicable Creative Commons License

the anomaly centers themselves are of great magnitude, which could potentially be due to the lower number of eddies within the composites. The observed anomalies are, largely, statistically insignificant relative to the background environment.

These results suggest a potential weakening of the spatial coherence between the eddy-associated SST anomalies and relevant analyzed variables as one tends toward the lower latitudes. This weakened response, particularly in the cloud and rain field, supports the work of Aguedjou et al. (2023), who found similarly weak anomalies in precipitation associated with mesoscale ocean eddies in the tropical Atlantic Ocean. We could attribute our results to the background SST characteristics of each region. As ocean currents at higher latitudes produce more pronounced SST gradients, the mesoscale ocean eddies formed have greater associated SST anomalies. These greater SST anomalies may induce a more robust, and statistically significant, response in the analyzed variables in the extratropics compared to regions such as the Maritime Continent (H. Liu et al., 2018).

Even though we identify a robust signal in the SST and surface heat flux anomalies in the Maritime Continent, these anomalies may be too weak to affect the atmosphere instantaneously or on shorter timescales in a similar vein as seen for the extratropics. In a numerical modeling study, Skyllingstad et al. (2019) had to artificially input a 3 K SST anomaly 500 km in width, relative to an ocean of homogeneous background SST, for there to be a response in the formation of tropical convection. These anomalies are much greater than the SST anomalies and sizes associated with eddies in the Maritime Continent. We also observed faster propagation rates of eddies within the Maritime Continent (Figures 3g and 3h), which may additionally reduce the likelihood of an instantaneous atmospheric response. However, preliminary analysis conducted through recategorization of eddies in the Maritime Continent by the propagation rate did not show sufficient evidence to support this hypothesis (not shown).

Several studies within and near the Kuroshio Extension identified that impacts of eddies on the atmospheric boundary layer, such as through vertical velocity and wind, may only reach 800–900 hPa (e.g., Ma et al., 2016; B. Sun et al., 2022). Our results suggest moistening (drying) of the column over warm-core (cold-core) eddies in the Kuroshio Extension and South China Sea, with potential increases (reductions) in cloud primarily in the Kuroshio Extension. The magnitude of the anomalies however suggest a relationship with shallow convection, compared to deeper convection. Rainfall anomalies associated with extratropical eddies have been observed to exceed 0.2 mm day^{-1} which, in regions such as the Southern Ocean, explain only a small portion of the variance (Frenger et al., 2013).

Initial analysis (not shown) found minimal vertical response in the atmosphere to eddies in the Maritime Continent, beyond the surface anomalies as shown in Figures 5–7. While it is therefore unlikely for eddies to affect rainfall patterns significantly in tropical regions such as the Maritime Continent, which experience much more rainfall all-year round, the magnitude of anomalies in rain and moisture even in the extratropics are still very small, as shown here. Therefore, it should be acknowledged that though anomalies appear more significant toward the extratropics, there remains a generally weak instantaneous response beyond the lowermost portion of the atmosphere.

While Aguedjou et al. (2023) find a generally minimal atmospheric response to mesoscale ocean eddies across the tropical Atlantic and Roman-Stork et al. (2021) note a weak response in the Bay of Bengal, Gulakaram et al. (2018) find a potential lag between eddies at peak amplitude and anomalies in the Bay of Bengal. However, in follow-up work (Gulakaram et al., 2023), relationships are suggested to be blurred by feedbacks on intra-seasonal timescales. Souza et al. (2021) conducted case study analyses in the Brazil-Malvinas Confluence, identifying a clear response to eddies only when transient atmospheric systems were stable, removing potential intraseasonal variability. The importance of intraseasonal variability in modulating the atmospheric response to eddies was also highlighted by Roman-Stork et al. (2021). The signal we observe in the Maritime Continent may also be weaker than in the extratropics as the precipitation is more convective, sporadic, and variable in nature, which may not be well resolved in the data used. Therefore, a coherent and statistically significant response, especially one that is instantaneous, in the Maritime Continent, is unlikely being a region with such high amplitude atmospheric variability, influenced by many processes particularly at intraseasonal scales.

5. Conclusion

In this study, we have used satellite altimetry data to detect and track eddies over a large domain including the Maritime Continent. We observe reductions in the number, mean peak amplitude, and duration of eddies, and increases in the propagation rate, at lower latitudes compared to higher latitudes, consistent with other studies.

21698996, 2025, 4, Downloaded from https://agupubs.onlinelibrary.wiley.com/doi/10.1029/2024JD042606 by University Of East Anglia, Wiley Online Library on [13/02/2025]. See the Terms and Conditions (https://onlinelibrary.wiley.com/terms-and-conditions) on Wiley Online Library for rules of use; OA articles are governed by the applicable Creative Commons License

Eddy hotspots, compared to the surrounding environment, were observed particularly where prominent currents interact, such as in the Kuroshio Extension and at the inflow of the Indonesian Throughflow.

By constructing normalized eddy composites, we identify the strongest eddy-associated sea surface temperature anomalies in the Kuroshio Extension, used as an extratropical case study. Surface heat flux and wind divergence anomalies in the Kuroshio Extension are also the greatest in magnitude, and significantly different from the background environment. Column water vapor, cloud liquid water, and rain anomalies associated with the eddies are spatially coherent with sea surface temperature anomalies, and statistically significant relative to the background environment, though are small in value.

However, anomalies associated with eddies in the Maritime Continent weaken closer to the equator. In the South China Sea, southeast tropical Indian Ocean, and Sulawesi Sea, eddies still show significant surface heat flux and wind divergence anomalies, spatially coherent with the sea surface temperature anomaly. For the South China Sea, there are also observable responses in column water vapor and cloud liquid water, but no detectable rain anomaly. Neither the southeast tropical Indian Ocean or Sulawesi Sea show distinct or coherent responses in these three anomalies. All three regions, in general, show atmospheric response, which lean toward statistical insignificance when compared to the background environmental variability.

These results suggest that latitudinal changes to the eddy-averaged sea surface temperature anomaly, dependent on the background sea surface temperature, are driving the responses noted. With the resultant enhanced heat flux and wind divergence anomalies associated with eddies in the extratropics, eddies are more likely to influence instability in the extratropical atmospheric boundary layer through modifications of column moisture, compared to tropical regions such as the Maritime Continent. These instabilities could alter the likelihood of cloud formation and rainfall. However, it should be noted that while the signal within the Maritime Continent may not be as strongly captured due to the nature of convection in terms of spatiotemporal variability, the faster propagation rates of eddies likely restrict an instantaneous response in the atmosphere from being as visible, which remains an open hypothesis to explore.

While the usage of a longer time period of analysis than existing studies allows compositing of a larger number of eddies, this analysis is limited to the instantaneous atmospheric response. In reality, part of the response may be associated with spatial variability and potential lead-lag relationships. To better realize the finer details regarding air-sea interactions associated with mesoscale ocean eddies, case studies using observational data and analysis of high-resolution model simulations would be required.

Future studies could consider the influence that other processes, which contribute to atmospheric variability in the Maritime Continent, have on the observed response to the eddies. The extent to which, for example, transient weather systems, larger-scale modes of variability, and the background environment in general affect composited responses, as shown in studies focusing on other regions, could then be highlighted and better understood. Evaluating the influence of these eddies on particular levels in the lower troposphere would give insight into the vertical structure of the atmospheric response, beyond the surface level. Such analysis would need data sets of higher vertical resolution, constrained in particular to the lowermost levels. Additionally, it would be worth assessing whether responses exist at finer scales, using high-resolution atmospheric simulations imposed with a background ocean containing eddies.

Nevertheless, our work has filled a gap in the literature related to the atmospheric response to eddies in the Maritime Continent. This study has highlighted a distinct difference between the Maritime Continent and the extratropics in both the characteristics of mesoscale ocean eddies and their associated interactions with the atmosphere. Our results will contribute to better understanding the role of the ocean in influencing the stability of the atmosphere in the Maritime Continent, particularly at the mesoscale, while also informing the degree of importance that representing and resolving ocean eddies in existing weather and climate models holds.

Data Availability Statement

Data sets used in this research are available through the following links: ERA5 (https://cds.climate.copernicus.eu/, last accessed on 13 Feb 2024) and DUACS AVISO ADT (https://marine.copernicus.eu/, last accessed on 7 Feb 2024). Documentation regarding the py-eddy-tracker algorithm of Mason et al. (2014) can be found through the

following Zenodo link (https://doi.org/10.5281/zenodo.7197432, courtesy of Delepoulle et al. (2022), last accessed on 7 Feb 2024).

Acknowledgments
Aslam was funded by NERC through a SENSE CDT studentship (NE/T00039X/1). Schwendike was partially funded by the Forecasting for Southeast Asia (FORSEA) project, funded by the Met Office Weather and Climate Science for Service Partnership (WCSSP) Southeast Asia, as part of the Newton Fund. Peatman and Birch were funded through the TerraMaris project (NE/R016739/1). Matthews was partially funded through the TerraMaris project (NE/R016704/1). This work was undertaken on ARC4, part of the High Performance Computing facilities at the University of Leeds, UK. The authors thank three anonymous reviewers for their comments on this paper.

References

Aguedjou, H. M. A., Chaigneau, A., Dadou, I., Morel, Y., Baloïtcha, E., & Da-Allada, C. Y. (2023). Imprint of mesoscale eddies on air-sea interaction in the Tropical Atlantic Ocean. *Remote Sensing*, *15*(12), 3087. https://doi.org/10.3390/rs15123087

Bôas, A. B. V., Sato, O. T., Chaigneau, A., & Castelão, G. P. (2015). The signature of mesoscale eddies on the air-sea turbulent heat fluxes in the South Atlantic Ocean. *Geophysical Research Letters*, *42*(6), 1856–1862. https://doi.org/10.1002/2015GL063105

Chelton, D. B., Schlax, M. G., Freilich, M. H., & Milliff, R. F. (2004). Satellite measurements reveal persistent small-scale features in ocean winds. *Science*, *303*(5660), 978–983. https://doi.org/10.1126/science.1091901

Chelton, D. B., Schlax, M. G., & Samelson, R. M. (2011). Global observations of nonlinear mesoscale eddies. *Progress in Oceanography*, *91*(2), 167–216. https://doi.org/10.1016/j.pocean.2011.01.002

Chelton, D. B., Schlax, M. G., Samelson, R. M., & de Szoeke, R. A. (2007). Global observations of large oceanic eddies. *Geophysical Research Letters*, *34*(15). https://doi.org/10.1029/2007GL030812

Chen, B., Xie, L., Zheng, Q., Zhou, L., Wang, L., Feng, B., & Yu, Z. (2020). Seasonal variability of mesoscale eddies in the Banda Sea inferred from altimeter data. *Acta Oceanologica Sinica*, *39*(12), 11–20. https://doi.org/10.1007/s13131-020-1665-2

Chen, G., Chen, X., & Cao, C. (2022). Divergence and dispersion of global eddy propagation from satellite altimetry. *Journal of Physical Oceanography*, *52*(4), 705–722. https://doi.org/10.1175/JPO-D-21-0122.1

Cheng, Y. H., Ho, C. R., Zheng, Q., & Kuo, N. J. (2014). Statistical characteristics of mesoscale eddies in the North Pacific derived from satellite altimetry. *Remote Sensing*, *6*, 5164–5183. https://doi.org/10.3390/rs6065164

Delcroix, T., Chaigneau, A., Soviadan, D., Boutin, J., & Pegliasco, C. (2019). Eddy-induced salinity changes in the Tropical Pacific. *Journal of Geophysical Research: Oceans*, *124*(1), 374–389. https://doi.org/10.1029/2018JC014394

Delepoulle, A., evanmason, Clément, CoriPegliasco, Capet, A., Troupin, C., & Koldunov, N. (2022). Antsimi/py-eddy-tracker: v3.6.1 (v3.6.1) [Software]. *Zenodo*. https://doi.org/10.5281/zenodo.7197432

Ffield, A., & Gordon, A. L. (1996). Tidal mixing signatures in the Indonesian seas. *Journal of Physical Oceanography*, *26*(9), 1924–1937. https://doi.org/10.1175/1520-0485(1996)026<1924:tmsiti>2.0.co;2

Frenger, I., Gruber, N., Knutti, R., & Münnich, M. (2013). Imprint of Southern Ocean eddies on winds, clouds and rainfall. *Nature Geoscience*, *6*(8), 608–612. https://doi.org/10.1038/ngeo1863

Fu, L. L., Chelton, D. B., Traon, P. Y. L., & Morrow, R. (2010). Eddy dynamics from satellite altimetry. *Oceanography*, *23*, 15–25. https://doi.org/10.5670/oceanog.2010.02

Godfrey, J. S. (1996). The effect of the Indonesian throughflow on ocean circulation and heat exchange with the atmosphere: A review. *Journal of Geophysical Research*, *101*(C5), 12217–12237. https://doi.org/10.1029/95JC03860

Gordon, A. L. (2005). Oceanography of the Indonesian seas and their throughflow. *Oceanography*, *18*(4), 14–27. https://doi.org/10.5670/oceanog.2005.01

Gulakaram, V. S., Vissa, N. K., & Bhaskaran, P. K. (2018). Role of mesoscale eddies on atmospheric convection during summer monsoon season over the Bay of Bengal: A case study. *Journal of Ocean Engineering and Science*, *3*(4), 343–354. https://doi.org/10.1016/j.joes.2018.11.002

Gulakaram, V. S., Vissa, N. K., & Bhaskaran, P. K. (2023). Mesoscale eddies with anomalous sea surface temperature and its relation with atmospheric convection over the North Indian Ocean. *International Journal of Climatology*, *43*(7), 3094–3113. https://doi.org/10.1002/joc.8018

Halo, I., Penven, P., Backeberg, B., Ansorge, I., Shillington, F., & Roman, R. (2014). Mesoscale eddy variability in the southern extension of the East Madagascar Current: Seasonal cycle, energy conversion terms, and eddy mean properties. *Journal of Geophysical Research: Oceans*, *119*(10), 7324–7356. https://doi.org/10.1002/2014JC009820

Hao, Z., Xu, Z., Feng, M., Li, Q., & Yin, B. (2021). Spatiotemporal variability of mesoscale eddies in the Indonesian seas. *Remote Sensing*, *13*(5), 1–27. https://doi.org/10.3390/rs13051017

Hao, Z., Xu, Z., Feng, M., Zhang, P., & Yin, B. (2022). Dynamics of interannual eddy kinetic energy variability in the Sulawesi Sea revealed by OFAM3. *Journal of Geophysical Research: Oceans*, *127*(8). https://doi.org/10.1029/2022JC018815

Hausmann, U., & Czaja, A. (2012). The observed signature of mesoscale eddies in sea surface temperature and the associated heat transport. *Deep-Sea Research Part I Oceanographic Research Papers*, *70*, 60–72. https://doi.org/10.1016/j.dsr.2012.08.005

He, Q., Zhan, H., Cai, S., He, Y., Huang, G., & Zhan, W. (2018). A new assessment of mesoscale eddies in the South China Sea: Surface features, three-dimensional structures, and thermohaline transports. *Journal of Geophysical Research: Oceans*, *123*(7), 4906–4929. https://doi.org/10.1029/2018JC014054

Hersbach, H., Bell, B., Berrisford, P., Hirahara, S., Horányi, A., Muñoz-Sabater, J., et al. (2020). The ERA5 global reanalysis [Dataset]. *Quarterly Journal of the Royal Meteorological Society*, *146*(730), 1999–2049. https://doi.org/10.1002/qj.3803

Ismail, M. F. A., Ribbe, J., Arifin, T., Taofiqurohman, A., & Anggoro, D. (2021). A census of eddies in the tropical eastern boundary of the Indian Ocean. *Journal of Geophysical Research: Oceans*, *126*(6). https://doi.org/10.1029/2021JC017204

Jiang, Y., Zhang, S., ping Xie, S., Chen, Y., & Liu, H. (2019). Effects of a cold ocean eddy on local atmospheric boundary layer near the Kuroshio Extension: In situ observations and model experiments. *Journal of Geophysical Research: Atmospheres*, *124*(11), 5779–5790. https://doi.org/10.1029/2018JD029382

Jochum, M., & Potemra, J. (2008). Sensitivity of tropical rainfall to Banda Sea diffusivity in the Community Climate System Model. *Journal of Climate*, *21*(23), 6445–6454. https://doi.org/10.1175/2008JCLI2230.1

Koch-Larrouy, A., Lengaigne, M., Terray, P., Madec, G., & Masson, S. (2010). Tidal mixing in the Indonesian seas and its effect on the tropical climate system. *Climate Dynamics*, *34*(6), 891–904. https://doi.org/10.1007/s00382-009-0642-4

Kurian, J., Colas, F., Capet, X., McWilliams, J. C., & Chelton, D. B. (2011). Eddy properties in the California Current System. *Journal of Geophysical Research*, *116*(C8), C08027. https://doi.org/10.1029/2010JC006895

Lee, T., Fournier, S., Gordon, A. L., & Sprintall, J. (2019). Maritime Continent water cycle regulates low-latitude chokepoint of global ocean circulation. *Nature Communications*, *10*(1), 2103. https://doi.org/10.1038/s41467-019-10109-z

Lindzen, R. S., & Nigam, S. (1987). On the role of sea surface temperature gradients in forcing low-level winds and convergence in the Tropics. *Journal of the Atmospheric Sciences*, *44*(17), 2418–2436. https://doi.org/10.1175/1520-0469(1987)044<2418:otross>2.0.co;2

Liu, H., Li, W., Chen, S., Fang, R., & Li, Z. (2018). Atmospheric response to mesoscale ocean eddies over the South China Sea. *Advances in Atmospheric Sciences*, *35*(9), 1189–1204. https://doi.org/10.1007/s00376-018-7175-x

21698996, 2025, 4, Downloaded from https://agupubs.onlinelibrary.wiley.com/doi/10.1029/2024JD042606 by University Of East Anglia, Wiley Online Library on [13/02/2025]. See the Terms and Conditions (https://onlinelibrary.wiley.com/terms-and-conditions) on Wiley Online Library for rules of use; OA articles are governed by the applicable Creative Commons License

Liu, J., Chen, G., Han, G., & Zhang, B. (2021). An eddy perspective of global air-sea covariation. *Journal of Meteorological Research*, *35*(5), 882–895. https://doi.org/10.1007/s13351-021-1013-2

Liu, X., Chang, P., Kurian, J., Saravanan, R., & Lin, X. (2018). Satellite-observed precipitation response to ocean mesoscale eddies. *Journal of Climate*, *31*(17), 6879–6895. https://doi.org/10.1175/JCLI-D-17-0668.1

Liu, Y., Yu, L., & Chen, G. (2020). Characterization of sea surface temperature and air-sea heat flux anomalies associated with mesoscale eddies in the South China Sea. *Journal of Geophysical Research: Oceans*, *125*(4). https://doi.org/10.1029/2019JC015470

Ma, J., Xu, H., & Dong, C. (2016). Seasonal variations in atmospheric responses to oceanic eddies in the Kuroshio Extension. *Tellus, Series A: Dynamic Meteorology and Oceanography*, *68*(1), 31563. https://doi.org/10.3402/tellusa.v68.31563

Ma, J., Xu, H., Dong, C., Lin, P., & Liu, Y. (2015). Atmospheric responses to oceanic eddies in the Kuroshio Extension region. *Journal of Geophysical Research: Atmospheres*, *120*(13), 6313–6330. https://doi.org/10.1002/2014JD022930

Madden, R. A., & Julian, P. R. (1994). Observations of the 40–50-day tropical oscillation — A review. *Monthly Weather Review*, *122*(5), 814–837. https://doi.org/10.1175/1520-0493(1994)122<0814:ootdto>2.0.co;2

Makarim, S., Sprintall, J., Liu, Z., Yu, W., Santoso, A., Yan, X. H., & Susanto, R. D. (2019). Previously unidentified Indonesian Throughflow pathways and freshening in the Indian Ocean during recent decades. *Scientific Reports*, *9*(1), 7364. https://doi.org/10.1038/s41598-019-43841-z

Mason, E., Pascual, A., Gaube, P., Ruiz, S., Pelegrí, J. L., & Delepoulle, A. (2017). Subregional characterization of mesoscale eddies across the Brazil-Malvinas Confluence. *Journal of Geophysical Research: Oceans*, *122*(4), 3329–3357. https://doi.org/10.1002/2016JC012611

Mason, E., Pascual, A., & McWilliams, J. C. (2014). A new sea surface height-based code for oceanic mesoscale eddy tracking [Software]. *Journal of Atmospheric and Oceanic Technology*, *31*(5), 1181–1188. https://doi.org/10.1175/JTECH-D-14-00019.1

McGillicuddy, D. J. (2016). Mechanisms of physical-biological-biogeochemical interaction at the oceanic mesoscale. *Annual Review of Marine Science*, *8*(1), 125–159. https://doi.org/10.1146/annurev-marine-010814-015606

Melnichenko, O., Amores, A., Maximenko, N., Hacker, P., & Potemra, J. (2017). Signature of mesoscale eddies in satellite sea surface salinity data. *Journal of Geophysical Research: Oceans*, *122*(2), 1416–1424. https://doi.org/10.1002/2016JC012420

Mori, S., Jun-Ichi, H., Yamanaka, M. D., Okamoto, N., Murata, F., Sakurai, N., et al. (2004). Diurnal land-sea rainfall peak migration over Sumatera Island, Indonesian Maritime Continent, observed by TRMM satellite and intensive rawinsonde soundings. *Monthly Weather Review*, *132*(8), 2021–2039. https://doi.org/10.1175/1520-0493(2004)132<2021:dlrpmo>2.0.co;2

Nagai, T., Hibiya, T., & Syamsudin, F. (2021). Direct estimates of turbulent mixing in the Indonesian archipelago and its role in the transformation of the Indonesian throughflow waters. *Geophysical Research Letters*, *48*(6). https://doi.org/10.1029/2020GL091731

Napitu, A. M., Gordon, A. L., & Pujiana, K. (2015). Intraseasonal sea surface temperature variability across the Indonesian seas. *Journal of Climate*, *28*(22), 8710–8727. https://doi.org/10.1175/JCLI-D-14-00758.1

Nencioli, F., Dong, C., Dickey, T., Washburn, L., & Mcwilliams, J. C. (2010). A vector geometry-based eddy detection algorithm and its application to a high-resolution numerical model product and high-frequency radar surface velocities in the Southern California bight. *Journal of Atmospheric and Oceanic Technology*, *27*(3), 564–579. https://doi.org/10.1175/2009JTECHO725.1

Ni, Q., Zhai, X., Wang, G., & Marshall, D. P. (2020). Random movement of mesoscale eddies in the global ocean. *Journal of Physical Oceanography*, *50*(8), 2341–2357. https://doi.org/10.1175/JPO-D-19-0192.1

Pang, C., Nikurashin, M., Pena-Molino, B., & Sloyan, B. M. (2022). Remote energy sources for mixing in the Indonesian Seas. *Nature Communications*, *13*(1), 6535. https://doi.org/10.1038/s41467-022-34046-6

Park, K. A., Cornillon, P., & Codiga, D. L. (2006). Modification of surface winds near ocean fronts: Effects of Gulf Stream rings on scatterometer (QuikSCAT, NSCAT) wind observations. *Journal of Geophysical Research*, *111*(C3). https://doi.org/10.1029/2005JC003016

Pegliasco, C., Chaigneau, A., Morrow, R., & Dumas, F. (2021). Detection and tracking of mesoscale eddies in the Mediterranean Sea: A comparison between the Sea Level Anomaly and the Absolute Dynamic Topography fields. *Advances in Space Research*, *68*(2), 401–419. https://doi.org/10.1016/j.asr.2020.03.039

Pegliasco, C., Delepoulle, A., Mason, E., Morrow, R., Faugère, Y., & Dibarboure, G. (2022). META3.1exp: A new global mesoscale eddy trajectory atlas derived from altimetry. *Earth System Science Data*, *14*(3), 1087–1107. https://doi.org/10.5194/essd-14-1087-2022

Penven, P., Echevin, V., Pasapera, J., Colas, F., & Tam, J. (2005). Average circulation, seasonal cycle, and mesoscale dynamics of the Peru Current System: A modeling approach. *Journal of Geophysical Research*, *110*(C10), 1–21. https://doi.org/10.1029/2005JC002945

Purba, N. P., Faizal, I., Damanik, F. S., Rachim, F. R., & Mulyani, P. G. (2020). Overview of oceanic eddies in Indonesia seas based on the sea surface temperature and sea surface height. *World Scientific News*, *147*, 166–178.

Roman-Stork, H. L., Subrahmanyam, B., & Trott, C. B. (2021). Mesoscale eddy variability and its linkage to deep convection over the Bay of Bengal using satellite altimetric observations. *Advances in Space Research*, *68*(2), 378–400. https://doi.org/10.1016/j.asr.2019.09.054

Seo, H., O'Neill, L. W., Bourassa, M. A., Czaja, A., Drushka, K., Edson, J. B., et al. (2023). Ocean mesoscale and frontal-scale ocean–atmosphere interactions and influence on large-scale climate: A review. *Journal of Climate*, *36*(7), 1981–2013. https://doi.org/10.1175/jcli-d-21-0982.1

Skyllingstad, E. D., de Szoeke, S. P., & O'Neill, L. W. (2019). Modeling the transient response of tropical convection to mesoscale SST variations. *Journal of the Atmospheric Sciences*, *76*(5), 1227–1244. https://doi.org/10.1175/JAS-D-18-0079.1

Small, R. J., deSzoeke, S. P., Xie, S. P., O'Neill, L., Seo, H., Song, Q., et al. (2008). Air-sea interaction over ocean fronts and eddies. *Dynamics of Atmospheres and Oceans*, *45*(3–4), 274–319. https://doi.org/10.1016/j.dynatmoce.2008.01.001

Souza, R., Pezzi, L., Swart, S., Oliveira, F., & Santini, M. (2021). Air-sea interactions over eddies in the Brazil-Malvinas Confluence. *Remote Sensing*, *13*(7), 1335. https://doi.org/10.3390/rs13071335

Sprintall, J., Gordon, A. L., Koch-Larrouy, A., Lee, T., Potemra, J. T., Pujiana, K., & Wijffels, S. E. (2014). The Indonesian seas and their role in the coupled ocean-climate system. *Nature Geoscience*, *7*, 487–492. https://doi.org/10.1038/ngeo2188

Storer, B. A., Buzzicotti, M., Khatri, H., Griffies, S. M., & Aluie, H. (2022). Global energy spectrum of the general oceanic circulation. *Nature Communications*, *13*(1), 5314. https://doi.org/10.1038/s41467-022-33031-3

Sun, B., Li, B., Yan, J., Zhou, Y., & Zhou, S. (2022). Seasonal variation of atmospheric coupling with oceanic mesoscale eddies in the North Pacific Subtropical Countercurrent. *Acta Oceanologica Sinica*, *41*(10), 109–118. https://doi.org/10.1007/s13131-022-2022-4

Sun, W., An, M., Liu, J., Liu, J., Yang, J., Tan, W., et al. (2022). Comparative analysis of four types of mesoscale eddies in the Kuroshio-Oyashio extension region. *Frontiers in Marine Science*, *9*. https://doi.org/10.3389/fmars.2022.984244

Susanto, R. D., & Ray, R. D. (2022). Seasonal and interannual variability of tidal mixing signatures in Indonesian seas from high-resolution sea surface temperature. *Remote Sensing*, *14*(8), 1934. https://doi.org/10.3390/rs14081934

Taburet, G., Sanchez-Roman, A., Ballarotta, M., Pujol, M. I., Legeais, J. F., Fournier, F., et al. (2019). DUACS DT2018: 25 years of reprocessed sea level altimetry products [Dataset]. *Ocean Science*, *15*(5), 1207–1224. https://doi.org/10.5194/os-15-1207-2019

21698996, 2025, 4, Downloaded from https://agupubs.onlinelibrary.wiley.com/doi/10.1029/2024JD042606 by University Of East Anglia, Wiley Online Library on [13/02/2025]. See the Terms and Conditions (https://onlinelibrary.wiley.com/terms-and-conditions) on Wiley Online Library for rules of use; OA articles are governed by the applicable Creative Commons License

Wallace, J. M., Mitchell, T. P., & Deser, C. (1989). The influence of sea-surface temperature on surface wind in the Eastern Equatorial Pacific: Seasonal and interannual variability. *Journal of Climate*, *2*(12), 1492–1499. https://doi.org/10.1175/1520-0442(1989)002<1492:tiosst>2.0.co;2

Wang, X., Cheng, X., Liu, X., & Chen, D. (2021). Dynamics of eddy generation in the Southeast Tropical Indian Ocean. *Journal of Geophysical Research: Oceans*, *126*(3). https://doi.org/10.1029/2020JC016858

Wirasatriya, A., Susanto, R. D., Kunarso, K., Jalil, A. R., Ramdani, F., & Puryajati, A. D. (2021). Northwest monsoon upwelling within the Indonesian seas. *International Journal of Remote Sensing*, *42*(14), 5437–5458. https://doi.org/10.1080/01431161.2021.1918790

Xue, P., Malanotte-Rizzoli, P., Wei, J., & Eltahir, E. A. (2020). Coupled ocean-atmosphere modeling over the Maritime Continent: A review. *Journal of Geophysical Research: Oceans*, *125*(6). https://doi.org/10.1029/2019JC014978

Yang, G., Yu, W., Yuan, Y., Zhao, X., Wang, F., Chen, G., et al. (2015). Characteristics, vertical structures, and heat/salt transports of mesoscale eddies in the southeastern tropical Indian Ocean. *Journal of Geophysical Research: Oceans*, *120*(10), 6733–6750. https://doi.org/10.1002/2015JC011130

Zu, Y., Fang, Y., Sun, S., Yang, G., Gao, L., & Duan, Y. (2022). The seasonality of mesoscale eddy intensity in the Southeastern Tropical Indian Ocean. *Frontiers in Marine Science*, *9*. https://doi.org/10.3389/fmars.2022.855832

Zuo, H., Balmaseda, M. A., Mogensen, K., & Tietsche, S. (2018). *OCEAN5: The ECMWF ocean reanalysis system and its real-time analysis component* (Tech. Rep.). Technical Report 823. ECMWF.

21698996, 2025, 4, Downloaded from https://agupubs.onlinelibrary.wiley.com/doi/10.1029/2024JD042606 by University Of East Anglia, Wiley Online Library on [13/02/2025]. See the Terms and Conditions (https://onlinelibrary.wiley.com/terms-and-conditions) on Wiley Online Library for rules of use; OA articles are governed by the applicable Creative Commons License